AD-A014 434

REMOTE DIAGNOSTICS AND CORRELATION ANALYSIS FOR
PRAIRIE SMOKE

S. A. Bowhill, et al

Aeronomy Corporation

Prepared for:

Rome Air Development Center
Defense Advanced Research Projects Agency

July 1975

259092

ADA014434

RADC-TR-74-182
Final Technical Report
July 1975

REMOTE DIAGNOSTICS AND CORRELATION
ANALYSIS FOR PRAIRIE SMOKE

Aeronomy Corporation

Sponsored by
Defense Advanced Research Projects Agency
ARPA Order No. 1423

Approved for public release;
distribution unlimited.

The views and conclusions contained in this document are those of the
authors and should not be interpreted as necessarily representing the
official policies, either expressed or implied, of the Defense
Advanced Research Projects Agency or the U. S. Government.

Rome Air Development Center
Air Force Systems Command
Griffiss Air Force Base, New York 13441

D D C

RECEIVED
AUG 28 1975
RECEIVED
D

REPORT DOCUMENTATION PAGE		READ INSTRUCTIONS BEFORE COMPLETING FORM
1. REPORT NUMBER RADC-TR-74-182	2. GOVT ACCESSION NO.	3. RECIPIENT'S CATALOG NUMBER
4. TITLE *(and Subtitle)* REMOTE DIAGNOSTICS AND CORRELATION ANALYSIS FOR PRAIRIE SMOKE		5. TYPE OF REPORT & PERIOD COVERED Final Technical Report April 1973 – March 1974
		6. PERFORMING ORG. REPORT NUMBER N/A
7. AUTHOR(s) S. A. Bowhill E. K. Walton D. R. Ward		8. CONTRACT OR GRANT NUMBER(s) F30602-73-C-0178
9. PERFORMING ORGANIZATION NAME AND ADDRESS Aeronomy Corporation P O Box 2209, Station A Champaign IL 61820		10. PROGRAM ELEMENT, PROJECT, TASK AREA & WORK UNIT NUMBERS 62301E 14233003
11. CONTROLLING OFFICE NAME AND ADDRESS Defense Advanced Research Projects Agency 1400 Wilson Blvd Arlington VA 22209		12. REPORT DATE July 1975
		13. NUMBER OF PAGES 133
14. MONITORING AGENCY NAME & ADDRESS*(if different from Controlling Office)* Rome Air Development Center (OCSE) Griffiss AFB NY 13441		15. SECURITY CLASS. *(of this report)* UNCLASSIFIED
		15a. DECLASSIFICATION/DOWNGRADING SCHEDULE N/A

16. DISTRIBUTION STATEMENT *(of this Report)*

Approved for public release; distribution unlimited.

17. DISTRIBUTION STATEMENT *(of the abstract entered in Block 20, if different from Report)*

Same

18. SUPPLEMENTARY NOTES

RADC Project Engineer:
Richard W. Carman/OCSE

19. KEY WORDS *(Continue on reverse side if necessary and identify by block number)*

Heated F Layer
Morphology of Artificial Spread F

20. ABSTRACT *(Continue on reverse side if necessary and identify by block number)*

The disturbed ionospheric region produced by the Platteville heating transmitter facility has been studied by the use of orbital and geostationary satellite signals. It has been found that the modifier transmitter produces an ellipsoidal disturbed region with an e-folding radius of about 50 km. This region is centered at the height of maximum of the ionospheric layer and displaced about 30 km north of the transmitter. The disturbed region is made up of geomagnetic field-aligned irregularities, having e-folding radius normal
(Cont'd)

DD $_{1 \text{ JAN } 73}^{\text{FORM}}$ 1473   EDITION OF 1 NOV 65 IS OBSOLETE

to the magnetic field of 75 to 400 m (the larger values are at night). They drift with the neutral wind with velocities of 8 to 25 m/s. These disturbances cause scintillations as high as 25 percent in a VHF radio signal transmitted through it when the line of sight approaches the direction of the magnetic field.

REMOTE DIAGNOSTICS AND CORRELATION
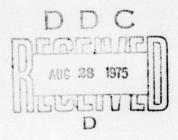# ANALYSIS FOR PRAIRIE SMOKE

S. A. Bowhill
E. K. Walton
D. R. Ward

ii

TABLE OF CONTENTS

1. INTRODUCTION

One of the major effects of the ionospheric heater is the production of artificial spread F (ASF). This phenomenon has been extensively studied by the transmission experiment.

1.1 Advantages of the transmission experiment

The transmission experiment is designed to study ASF by examining amplitude fluctuations from orbiting and geostationary satellite signals received at VHF and UHF by receivers spaced at fixed locations on the ground. The transmission experiment has the following advantages for the study of ionospheric irregularities:

1. The location of the transmitting satellite is accurately known, and the frequencies are sufficiently high for ionospheric refraction to be neglected; so the position of the line of sight (LOS) is accurately predetermined.

2. The ground receiving site can be located so that the LOS passes through any desired part of the disturbed volume.

3. Orbital satellites have a LOS that traverses the disturbed region so rapidly that internal motions of the plasma are negligible as a factor in producing amplitude scintillations.

4. For irregularities with correlation distances of 200 m or less, the fluctuations in phase, produced by passage of VHF waves through ASF, are fully developed into amplitude scintillations by the time they reach the ground, so that the phase scintillation fluctuation can be deduced from the depth of amplitude fluctuation.

5. The propagation of VHF and UHF waves through the disturbed region is of inherent interest for some propagation applications of ASF; for instance, degradation of radar tracking of orbiting or ballistic missiles.

1

1.2 Objectives of the transmission experiment

In planning the implementation of the transmission experiment, the following objectives were considered as needing to be determined by measurements of ASF irregularities:

1. Irregularity orientation--whether the ASF structure is aligned with the earth's magnetic field.

2. Irregularity size and shape--dimensions of the correlation ellipsoids associated with the various structure sizes present in the irregularities.

3. Altitude distribution--relative intensity of the electron-density fluctuations as a function of altitude in the disturbed region of the ionosphere.

4. Horizontal extent--large-scale horizontal variation of fluctuation intensity in the north-south and east-west directions.

5. Onset and decay--variations of the irregular structure with time when the heating transmitter is switched on or off.

6. Drift velocity--large-scale velocity of the irregularities due to gross motion of the ionospheric plasma.

7. Frequency variation--intensity and time scale of amplitude fluctuations of signal transmitted through the heated region as a function of wave frequency.

8. Multipath effects--occurrence of multipath scintillations or off-LOS scatter.

9. Yield studies--effects of transmitter parameters such as heater reflection height, power and modulation on the intensity of the electron-density fluctuations.

10. Radar simulation--simulation of scintillation effects anticipated during radar track of objects located behind the disturbed region.

1.3 Data processing

In processing the data from both the orbital and the geostationary satellites, it was necessary to take into account the modulation characteristics of the satellite signals. As part of a study to determine the effect of the satellite modulation on the data analysis, the spectra of both the orbital and geostationary signals were computed. The data available was the heterodyne tone generated by the receiver BFO and recorded on four-track analog magnetic tape. The recorded tone was directly digitized at a 12-kHz rate, and the resultant time series was transformed to the frequency domain by a fast Fourier transform. Although the modulation of the satellites was a type of phase pulse modulation, the bandwidth of the receiving system produced an amplitude modulation characteristic which can be seen in the resultant power spectral density plots in Figures 1.1 and 1.2. As can be seen, the geostationary signal (shifted by the heterodyning process to about 900 Hz) has sidebands about 200 Hz on either side. The orbital satellite has sidebands about 2.5 kHz on either side. These modulation characteristics caused no trouble in the processing of the geostationary satellite signal since the fastest scintillation time was on the order of a few seconds. The orbital satellite data, on the other hand, contain events in the millisecond range. This can cause considerable problems if the phase modulation on the satellite signal causes amplitude variations of the recorded (or detected) heterdyne tone.

Once the signal amplitude was properly detected, the processing of the data in terms of ASF scintillations could begin. Figure 1.3 shows the configuration available for a geostationary satellite. ASF irregularities form "shadows" on the ground plane that can be studied by suitably placed receiving antennas A, B, and C. Since all such satellites are located in the equatorial plane, their lines of sight are all somewhat to the south, so the three-station network must be offset from the center of the disturbed region in order to allow
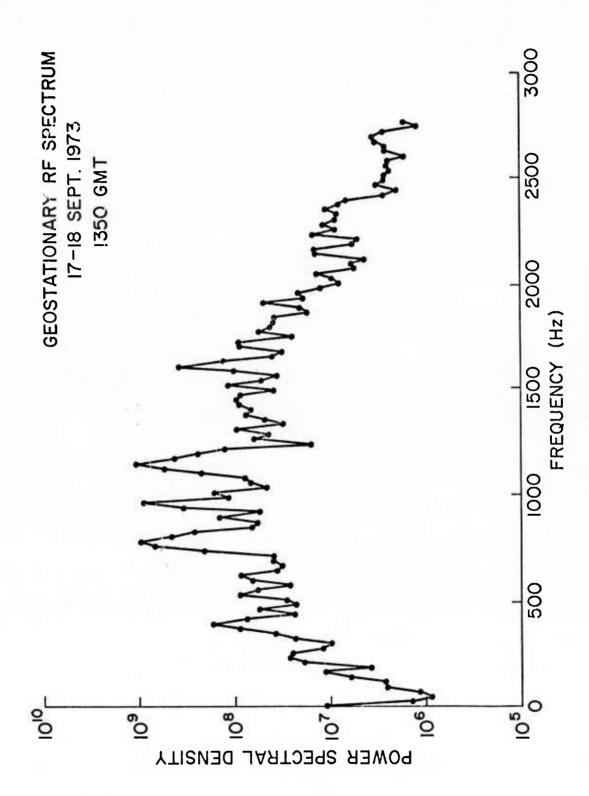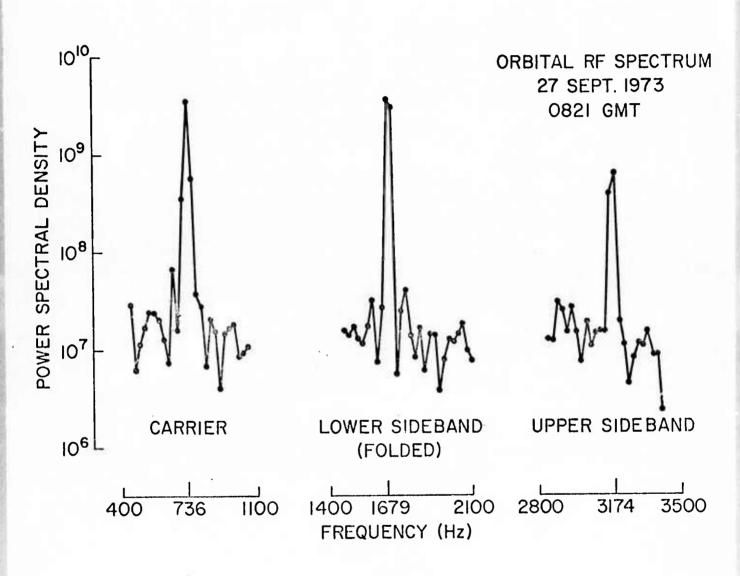
Figure 1.1 Geostationary RF spectrum
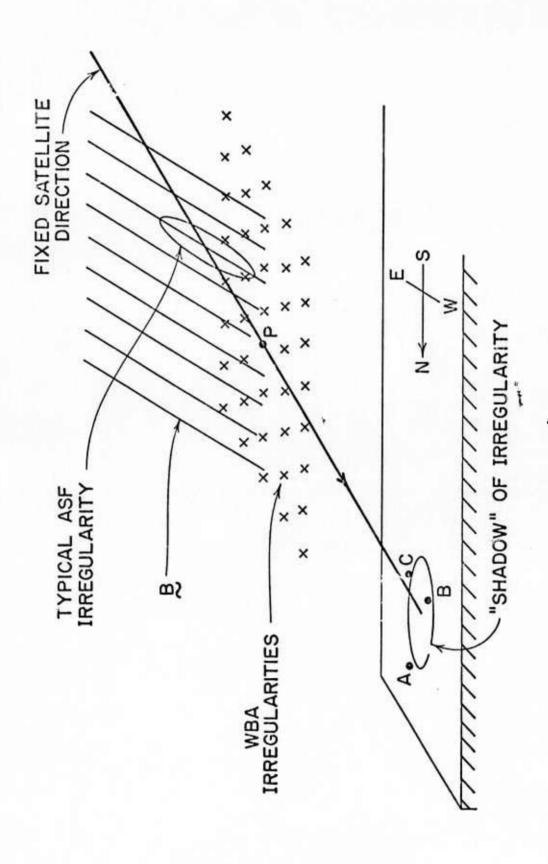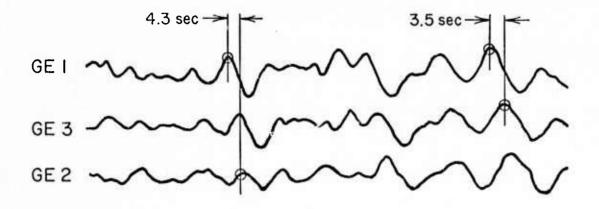
4

Figure 1.2 Orbital RF spectrum

Figure 1.3 Geostationary satellite configuration

observation of scintillations. Here, the line of sight is virtually stationary, so the observations obtained are complementary to the orbiting-satellite observations in that time variabilities in the medium are dominant.

The general character of the scintillation observations when the heater transmitter is on is illustrated in Figure 1.4. The autocorrelation function is nearly Gaussian in shape, the fading having an average period of about 10-15 sec. The unheated quiet ionosphere has a scintillation index S (see Section 4.2) of about 0.01, while values of S up to 0.25 have been observed for the heated ionosphere, depending on the heater power and frequency. It is evident that the fading pattern is nearly identical at the three receivers, but simply displaced in time by the amount shown. From this it is concluded that internal velocities in the ionospheric irregularities are negligible, and that the fading is due primarily to the drifting of elongated irregularities over the antenna triangle. These data were analyzed by correlation techniques to give the size of the structure observed at the ground, and the direction and magnitude of the velocity of the irregularities.
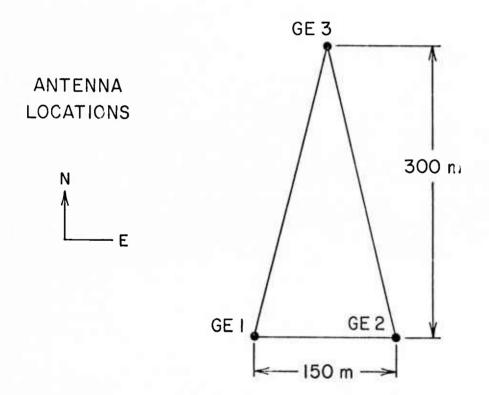
Figure 1.4 Illustrating time shifts between antennas in the geostationary experiment

2. REMOTE EXPERIMENT

2.1 Introduction

An ionospheric heater produces field-aligned ionization irregularities in the region of the ionosphere directly above it. It has been suggested (Bowhill, et al., 1971 pp 19-21) that these irregularities might propagate along the lines of the earth's magnetic field and appear as mirror image irregularities in the magnetically conjugate ionosphere; namely, at a region located over the same magnetic field line as the ionosphere over the heater transmitter, but in the southern hemisphere rather than the northern. The search for such an effect is known as the "remote experiment", and the conjugate point location is code named BOWATER. It will be so referred to in the remainder of this report.

The inaccessibility of BOWATER in the southern Pacific Ocean causes considerable difficulty in planning a diagnostic experiment; the F region over BOWATER is over the horizon from all land masses. It is in fact very close to the furthest point from land in the entire globe. Direct radar probing is therefore out of the question.

2.2 Aircraft experiment

The next possibility explored was an aircraft-borne diagnostic. An experiment carried out on March 29 and 31, 1971 (Bowhill, 1971 pp 29-32; Bowhill, et al., 1973) over the heater transmitter established that a properly instrumented airborne ionosonde could adequately probe for ASF. However, the aircraft used (provided by RADC) was heavily committed for an auroral-measurement program, and therefore was unavailable. The possibility was then explored (Bowhill, et al, 1973, pp 53-57) of using an aircraft provided by LASL, carrying a chirp ionosonde. It was ultimately decided that the multiple enroute refueling and the marginal performance of the chirp ionosonde made this approach impractical.

9

2.3 Satellite experiment

It was next decided to explore the use of a satellite-borne topside sounder for the detection of ASF, since such a sounder routinely crosses the latitude of BOWATER twice in each orbit. With the cooperation of Dr. Hartz of the Communications Research Centre, Ottawa, a successful experiment was made over Platteville on April 10, 1972 (Bowhill, et al. 1973, pp 35-39). A satellite experiment over BOWATER was therefore planned.

The first difficulty encountered was the remoteness of BOWATER from the nearest satellite readout station at Christchurch (the path PF on Figure 2.1). To be able to command the satellite transmitter on, it was necessary for the satellite to be at least 3000 km altitude above BOWATER in order to have an adequate elevation angle at Christchurch. Only two of the four orbiting top-side sounder satellites (Alouette II and ISIS I) have sufficiently elliptical orbits to permit this type of measurement, and as it turns out, only ISIS I gives adequate signal strength.

This experiment has the advantage that its passage over BOWATER is pre-dictable months in advance, permitting careful advanced planning. However, the following disadvantages of the experiment have become apparent:

1. The relative infrequency of suitable high-altitude passes makes it difficult to schedule the heater transmitter operation at exactly the right time, given the many other constraints on transmitter scheduling.

2. The high altitude of the satellite means that the ionospherically-reflected signal is about 15 dB down relative to that prevailing for its normal low-altitude operation. In addition, the ISIS I satellite antenna is tumbling, the net effect being a lack of returned signal for at least 50 percent of the time.
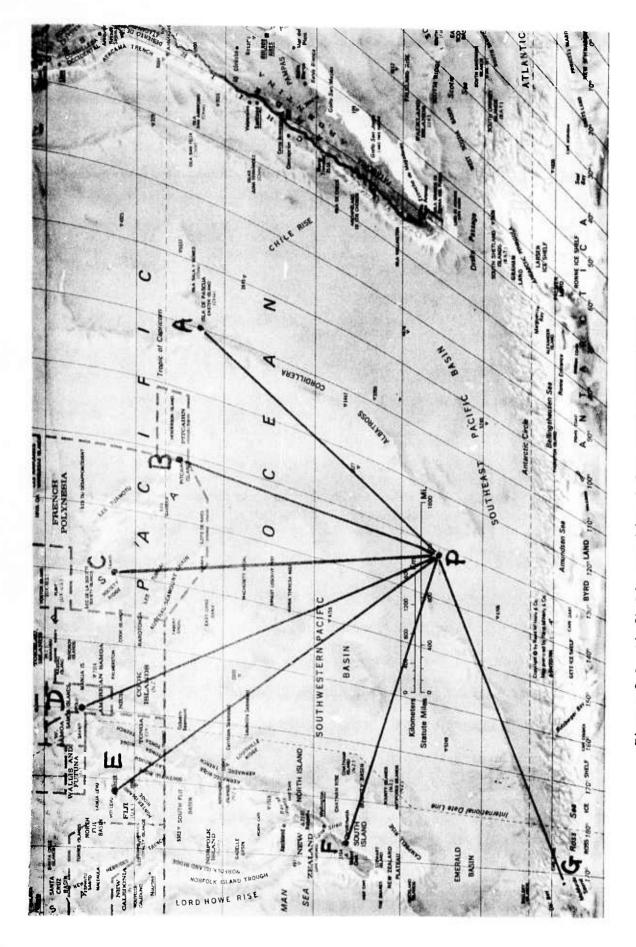
10

Figure 2.1 Airfields considered for Remote Experiment

3. The difficulty of operating the satellite under high-altitude
    conditions means a lack of an adequate data base to describe the
    properties of the ambient or undisturbed ionosphere.

4. It is found that high-altitude topside soundings at this latitude
    are strongly perturbed by ionospheric returns thousands of kilo-
    meters away from the subsatellite point.

Nevertheless, some interesting experimental results were obtained and
are described in the next section.

2.4 Experimental results

Parameters of five passes of the topside satellite ISIS I over BOWATER
were (taken as nominally 54.40S, 131.90W) are given in Table 2.1. The al-
titudes of passage varied from 3252 to 3538 km, and the maximum elevation
angles observed from a point at ground level varied from 87.1 to 89.8 deg.
For a satellite altitude of 3200 km, a maximum elevation angle of 89 deg cor-
responds to a satellite passage about 56 km to the east or west of the conjugate
point, indicating the difficulty of obtaining an exactly overhead pass. However,
it seems reasonable to expect that the disturbed region at the conjugate point
would extend over a region greater in diameter than the approximate 100-km
diameter of the heated region in the northern hemisphere, so some effect might
be expected to be seen even for maximum elevation angles as low as 87 deg.

Results of these various passes will now be described. The ionograms were
furnished by Dr. T. R. Hartz of CRC, Ottawa, and his cooperation has proved
invaluable in these investigations

2.4.1 Event A results

Figure 2.2 shows the position of the satellite to scale at 11 times during
its passage over BOWATER on February 22, 1973; the field line through BOWATER
is also indicated. Figure 2.3(a) through 2.3(k) show examples of the topside

12

Table 2.1

Events over selected earth points

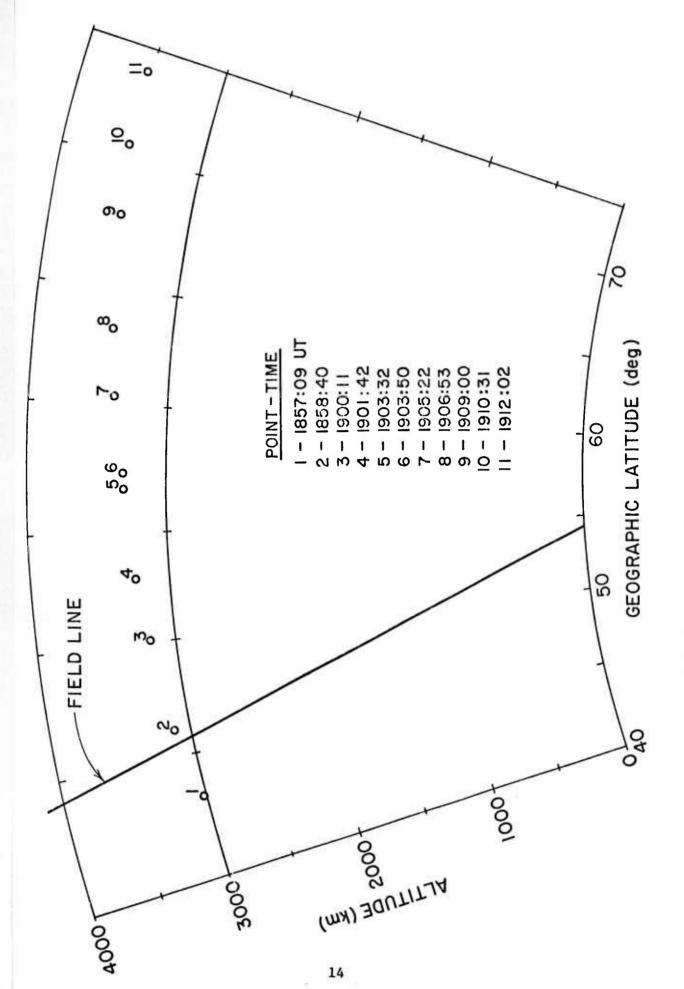| Event Code	Date(1973)	Closest Approach Time (UT)	Maximum Elevation Angle	Altitude (km)	Heater Power (Mw)
A	Feb 27	19:02:15	89.1	3252	1.6
B	Sept 3	05:22:54	89.8	3443	0
C	Sept 14	04:31:40	88.5	3538	.88-1.48
D	Sept 25	03:40:33	87.1	3336	0
E	Sept 30	03:28:47	88.5	3162	1.17

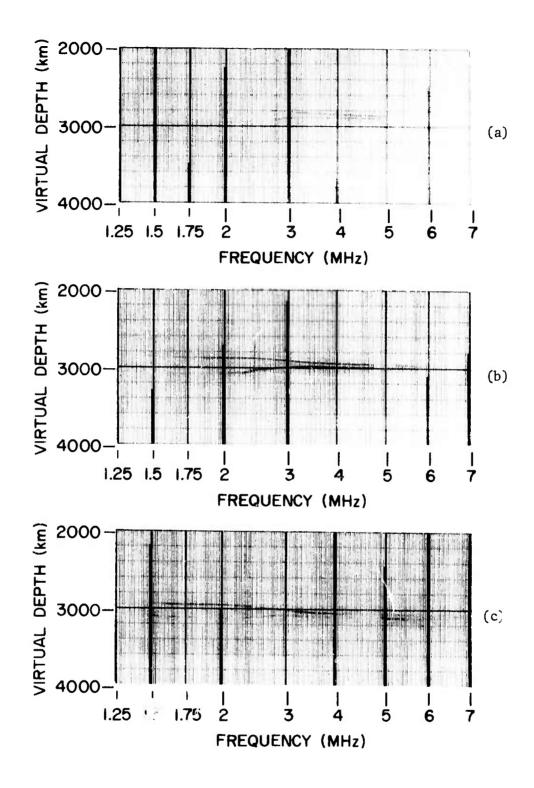Figure 2.2 Topside satellite locations

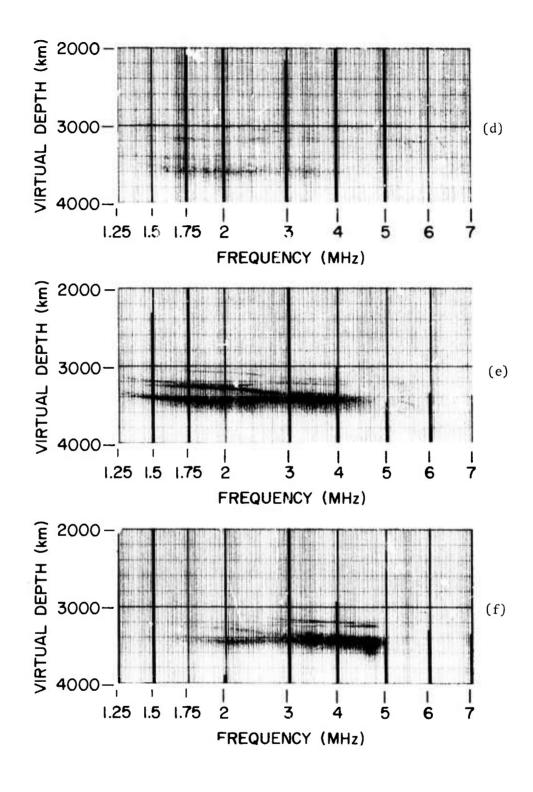Figure 2.3   Topside ionograms

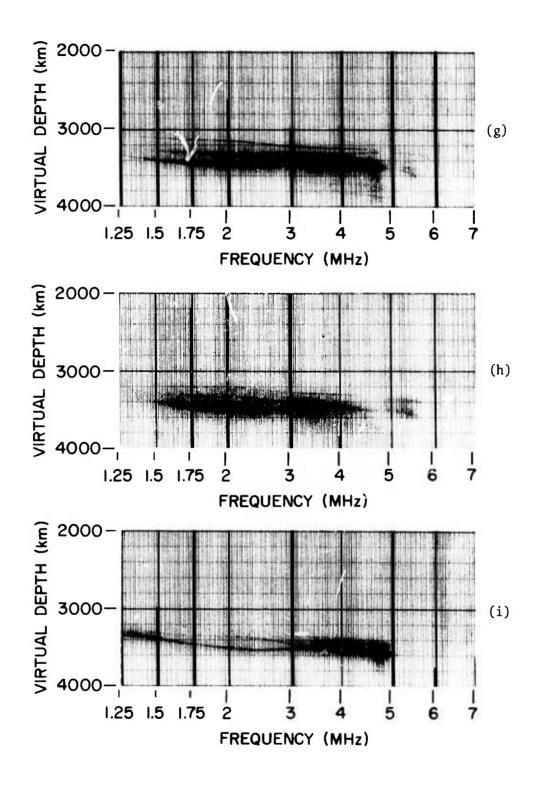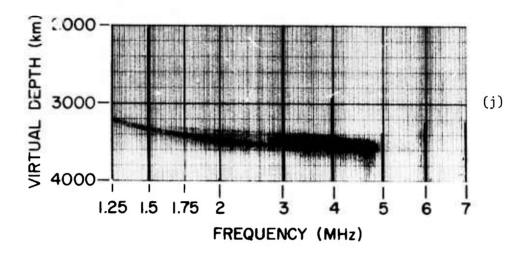15

Figure 2.3 Topside ionograms, Cont'd
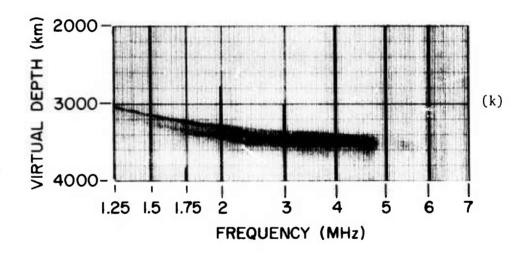
16

Figure 2.3 Topside ionograms, Cont'd

Figure 2.3 Topside ionograms, Cont'd

18

ionograms obtained when the sounder was at these 11 points. For clarity only the positions from 2000 to 4000 virtual depth and from 1.25 to 6 MHz frequency, are shown.

Particularly interesting is the ionogram corresponding to point 7, taken at 10:05:22 UT. This is reproduced in trace form on Figure 2.4. Three types of trace are visible:

1. Vertical-incidence reflections from the undisturbed topside ionosphere (labeled "A") on the ionograms;

2. Ducted echoes from field-aligned sheets of ionization (labeled "B" on the ionograms) having somewhat greater range than the "A" echoes but having a critical frequency (f_B) substantially less than the critical frequency (f_A) of the "A" echoes due to the obliquity of the incidence;

3. An even longer-range trace ("C" on the ionograms) which arises from orthogonal backscatter from field-aligned irregularities in the top-side ionosphere.

It is noticeable that echoes of type "A" and "B" are present throughout the ionogram sequence, while echoes of type "C" are visible in appreciable amounts only at point 7 on Figure 2.2. Scatter of this type is not a usual feature of topside ionograms in this latitude range. It is therefore concluded that the field-aligned scatter observed at BOWATER on this occasion was probably produced by field-aligned structure originating from the heater transmitter in the northern hemisphere.

2.4.2 Events B and D results

During the Prairie Smoke V field exercise, it was possible to schedule four passes (Events B through E) when the heater transmitter was thought to be available. In September 1973, the high passes of ISIS I over BOWATER were all
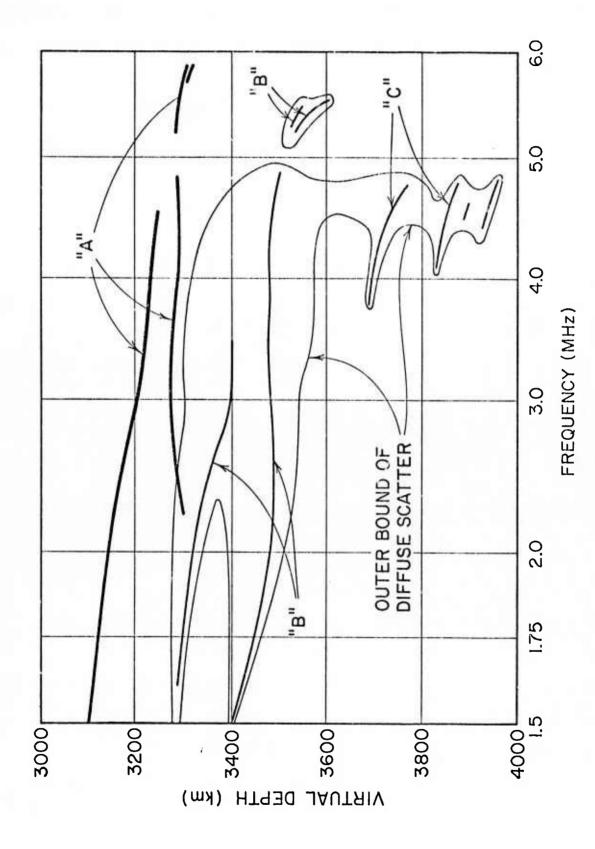
Figure 2.4   Magnified sketch of a portion of a topside ionogram

in the late evening, postsunset, (1900-2030 BOWATER time) as opposed to Event A in which the passes were in the late morning (1000 BOWATER time). Only on two of these events (C and E) was it possible to schedule heater transmitter operation; for Events B and D, heater transmitter operation was not available, so these were to act as a "control" indicating ambient conditions in the absence of heating.
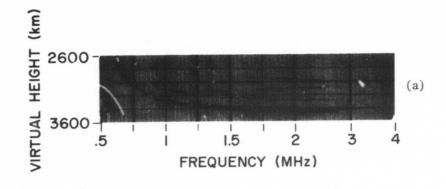
The leading feature of the ionograms taken in this event is the extreme complexity of the returned echoes, indicated on Figures 2.5(a) through 2.5(c). Figure 2.5(a) shows an ionogram from Event D taken close to overhead BOWATER; the satellite was at a height of 3336 km. In addition to the main echo at about 3400-km altitude, additional returns are visible at 2 MHz frequency and virtual depths from 2970 to 3280. The echo at 2970-km virtual depth (370 km short of ground range) indicates that the F layer was at a very high altitude at that time. The stronger echoes probably result from field-aligned reflections corresponding to those indicated at "B" on Figure 2.4.
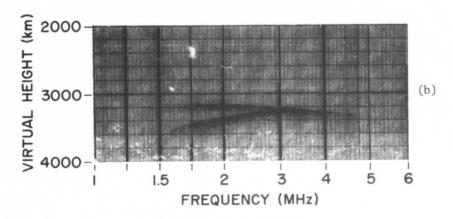
In Event B, a quite different type of behavior was seen. While only fractions of the traces are available due to antenna pattern problems, the ionogram shown in Figure 2.5(b), corresponding to nearly overhead BOWATER, shows quite disturbed traces with up to 200 km range spreading. Figure 2.5(c), taken at a point corresponding in position to point 7 on Figure 2.2, shows even greater spreading and many apparently distinguishable traces.

This quite different behavior of the late evening ionosphere observed at very high altitudes over BOWATER makes it quite difficult to place Events C and E (for which heating was available) in proper perspective.

2.4.3 Event C results

On September 14, 1973, at 04:31:40, the ISIS I satellite passed very nearly overhead BOWATER (88.5 deg maximum elevation angle) at an altitude of 3538 km, and the Platteville heater was operating at 2.85 MHz with a power that was

21

Figure 2.5 Topside ionograms

varying (in the immediate time of passage) from .88 to 1.48 Mw. The F2-layer critical frequency at Erie (near Platteville) was 3.8 MHz, and strong spread F was observed.

Figure 2.6 shows a composite ionogram made from three frames of the sounder at 04:29:31, 04:29:49 and 04:30:07. Since none of the three frames shows a complete ionogram, the three have been combined in five frequency ranges into a single composite ionogram displaying the clearest traces in each. During this time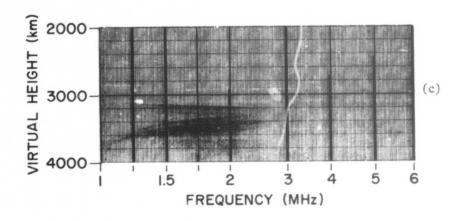 the satellite was very close to apogee, and its altitude did not vary by more than 5 km during the time of these three ionograms. A diffuse trace is seen with a minimum range of about 3500 km (thereby precluding its being an echo reflected from the topside of the ionosphere, ducted along the magnetic field). In addition, two "hard" traces are seen at shorter ranges, one at only 3300 km range. These additional traces are not visible when the satellite has passed to the south of BOWATER, and it seems likely that they were produced by irregularities in that general vicinity.

2.4.4 Event E results

On September 30, 1973, the satellite ISIS I passed over BOWATER at 03:28:47 UT, with a maximum elevation angle of 88.5 deg and an altitude of 3162 km. At that time the Platteville heater was radiating at 1.17 Mw power, at a frequency of 2.855 MHz. The critical frequency of the F2 layer measured at Erie was 4.2 MHz and a strong spread F was observed.

The general behavior of the ionogram when the satellite was overhead BOWATER is sketched on Figure 2.7(a) though actual ionograms are not shown since they were of poor quality. Well-defined vertical and oblique returns are visible, the ratio of the ranges corresponding to the inclination of the magnetic field.

In the neighborhood of the point corresponding to point 7 on Figure 2.2, the appearance of the ionograms was as sketched on Figure 2.7(b) showing
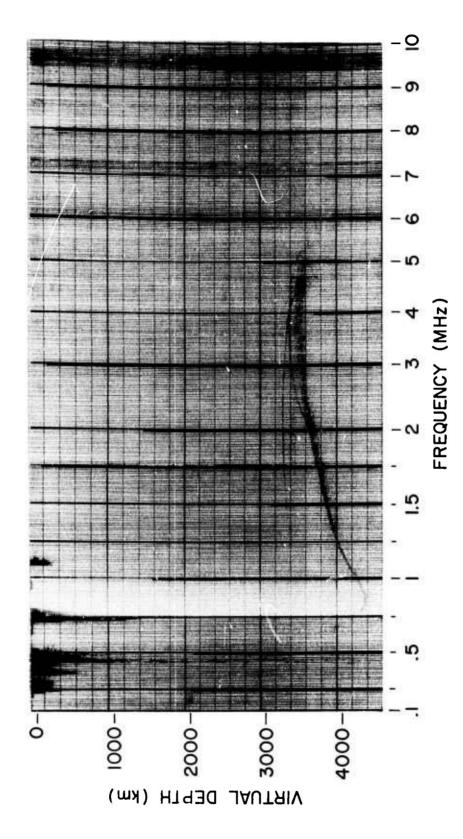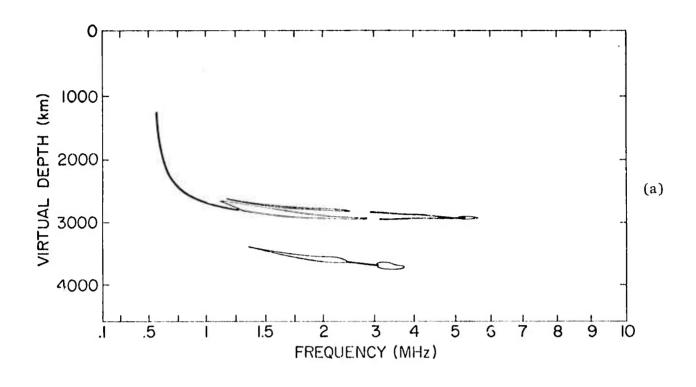
Figure 2.6 Composite topside ionogram

24
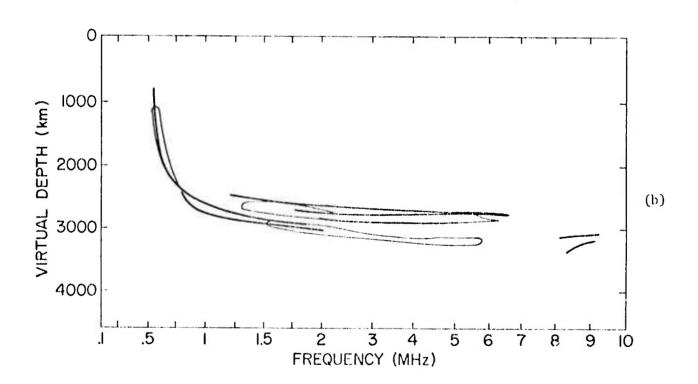
Figure 2.7 Sketches of composite topside ionograms

25

marked spread between the O and X traces, but nothing that could be directly attributed to scattering from the vicinity of BOWATER.

2.5 Discussion

The conclusion drawn from a study of these results is that the daytime behavior (illustrated by Event A) showed interesting phenomena that might be attributed to heating of the conjugate ionosphere. However, the available satellites at the end of the Prairie Smoke V exercise offered only night passes, where the appearance of the ionograms was extremely variable from night-to-night. Therefore, it is felt that no clear picture as to reality of the conjugate effect emerged from the Prairie Smoke V results. The following recommendations have been made for resolution of this matter:

1. Use of a ground-based diagnostic in the location of BOWATER, capable of continuous measurements; for example, a nuclear-submarine-mounted geostationary and orbital satellite-scintillation measuring system, similar to that used successfully at Platteville.

2. Carefully preprogrammed cyclical sequences of heating experiments covering both day and night conditions at Platteville, accompanied by radio-silent measurements at BOWATER of the kind indicated above.

3. Analysis of the results to determine the spatial extent and intensity of the perturbations and the coincidence of occurrence with heating at Platteville.

3. CORRELATION ANALYSIS

3.1 Introduction

Much of the data received during the Prairie Smoke transmission experiments may be used to determine the velocity, size and orientation of the structures which comprise the disturbed region. Time variations were studied using the geostationary ATS-5 satellite, and spatial variations were studied using the orbital Navy navigation satellites.

3.2 Geostationary velocity analysis

The geostationary observation station, essentially the same as used in Prairie Smoke IV, was used to receive the 136 MHz transmission from ATS-5. The station was located (in Lusk, Wyo.) so that the LOS to the geostationary satellite passed over the Platteville heater at 275 km. The signal used in this study was received and mixed with the local receiver BFO for recording on an audio tape recorder with time from WWV. The beat note was also detected, filtered, digitized, and stored on digital magnetic tape for later analysis. This is the same technique used in Prairie Smoke IV.

These digital signal amplitude records were analyzed using auto- and cross correlation techniques. Figure 3.1 shows an example of the correlations for the east-west antenna pair. It is possible to compute the velocity of the interference pattern from these correlations using the "straight-line" technique of Briggs, et al.(1950). This technique takes into account both the drift velocity of the pattern produced by the irregularities as well as random changes in the shape of the pattern itself. The following equation is developed in Briggs, et al. (1950):

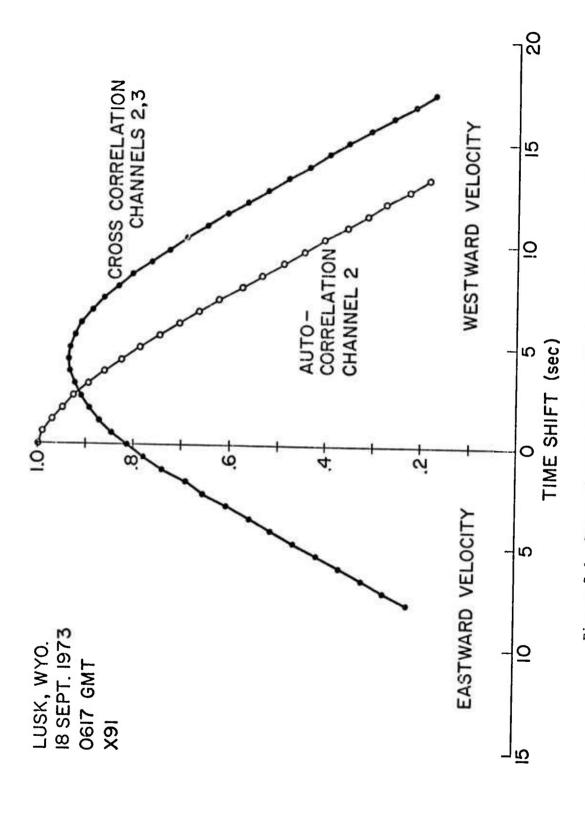$$\tau'^2 - \tau^2 = \frac{\xi_0^2}{V_R'^2} - 2\frac{\xi_0 V_D}{V_R'^2}\tau$$

27

Figure 3.1 Geostationary correlation for 18 September 1973

where

τ = cross correlation time shift

τ' = autocorrelation time shift (τ and τ' taken at equal correlation magnitudes)

ξ_0 = antenna spacing

V'_R = "fading" velocity

V_D = steady drift velocity

Note this is the equation of a straight line in $\tau'^2 - \tau^2$ versus τ space. Figure 3.2 is a plot of these parameters taken from Figure 3.1. As can be seen, these data points form (essentially) a straight line. The slope and intercept of this straight line can be used to find the two velocities shown in the equation above. Using this procedure, the steady drift velocity is found to be 35.3 m/sec and the "fading" velocity is 41 m/sec (these are westward velocities; the north-south velocities have been found to be essentially zero). Briggs, et al.(1950) show that an apparent velocity (V_R) due to random variations in the shape of the (drifting) pattern may be calculated from

$$V_R'^2 = V_P^2 + V_R^2 .$$

Application of this equation gives V_R = 20.8 m/s for the example.

The majority of the data were not analyzed in this way. The velocity was deduced from the time shift of the peak of the cross correlation curves. A comparison of this technique with the more complete Briggs, et al.(1950) straight line may be made in this example. Taking the time shift of the peak as 4.5 sec, the velocity is calculated as 41 m/sec. This velocity is the same as the "fading" velocity as calculated earlier, only slightly larger than the actual steady drift velocity (35.3 m/sec). The discrepancy is due to the effect of the random change of shape of the pattern as it drifts. It is necessary to keep this discrepancy
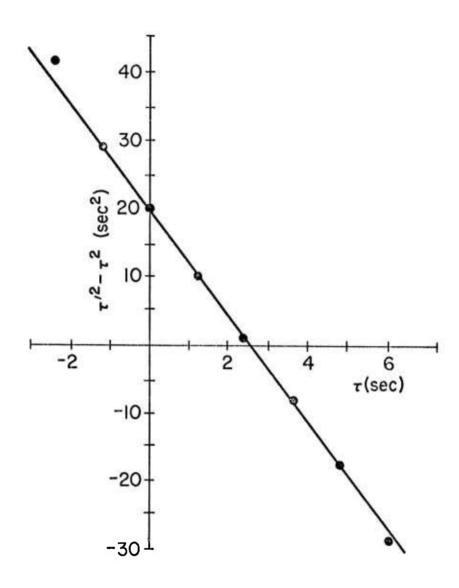
Figure 3.2 Briggs, Phillips, and Shinn straight line

in mind when considering the velccity magnitudes in the next section. They are quite likely inflated slightly by the random variations in the pattern shape.

Information about the characteristics of the heated region can be obtained from the velocity of these irregularities across the spaced antenna system (Bowhill and Ward, 1973a). From this velocity, the apparent structure size in the heated region can be obtained. For obtaining these quantities, recordings made on the nights of 17, 18, 19 September 1973 were chosen because these records are continuous and can be compared with previous daytime results.

The velocities for the three nighttime runs are shown in Figures 3.3, 3.4, and 3.5. The velocity shows a westward dominance but it occasionally changes to east with no apparent dependence on time. There also seems to be a wide variation in the magnitude of the velocity. The e^{-1} structure sizes were calculated from these velocities and sorted to determine the frequency of occurrence. In Figure 3.6 the daytime results are given and Figure 3.7 shows the distribution of nighttime results obtained in Prairie Smoke IV. There is a clear separation in the sizes where larger structures ($\sim$350 m) are seen more frequently at night and smaller structures ($\sim$100 m) in the day. These systematic differences between night and day could be caused by the LOS passing through a different part of the region from day to night.

3.3 Geostationary correlation data

As an example of the geostationary yield analysis, a computer output is shown in Figures 3.8 and 3.9. These two figures contain auto- and cross correlation information for three channels of geostationary data over a 30-minute period. The computer prints "DATAFILE, INTERVAL" and awaits response by an operator or punched paper tape. The "X910@@" is the name under which the data are stored and "Ø2" is the increment of time shift (T) which is used in the correlation calculation. From this point the output is generated by the computer as a result of calculations. The 30-minute interval is divided into six 5-minute parts numbered in the figures.
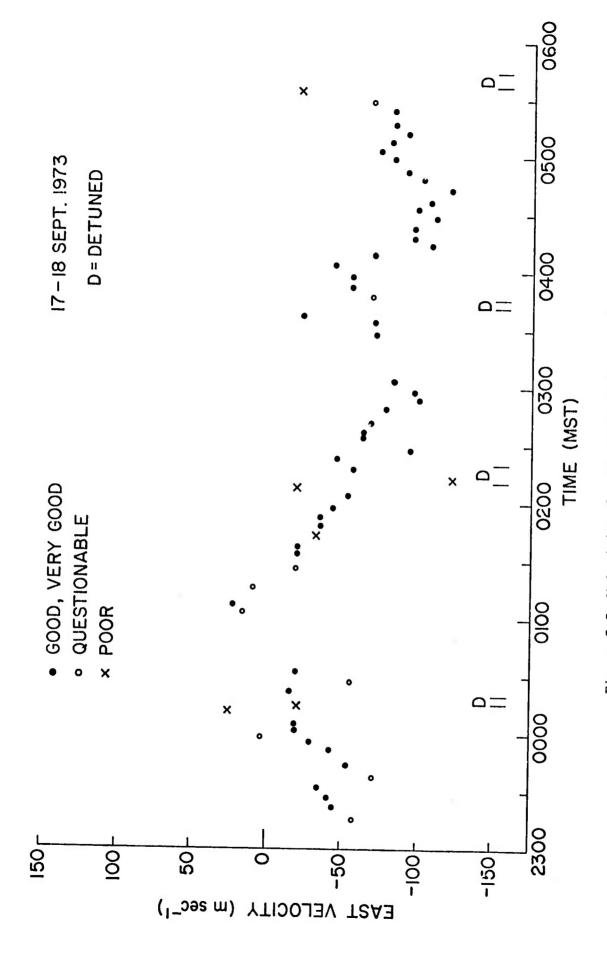
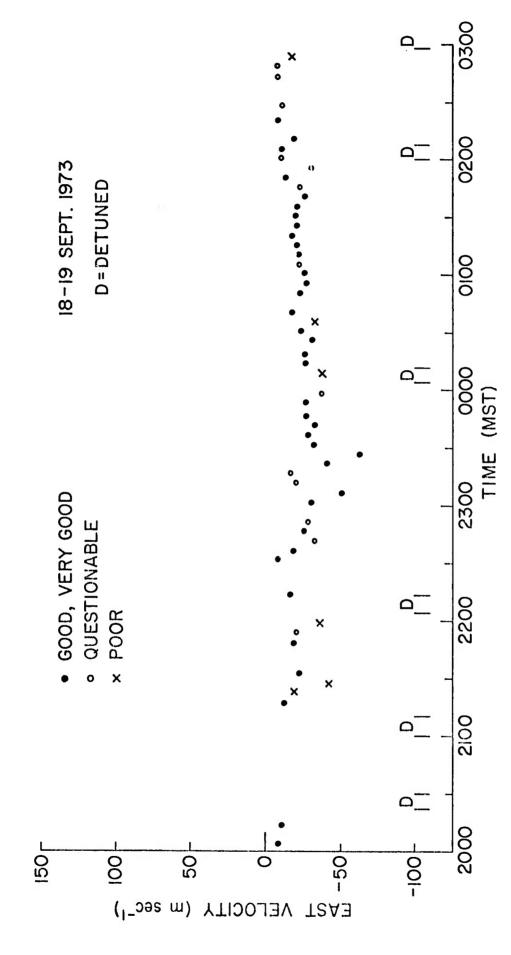Figure 3.3 Velocities for 17-18 September 1973
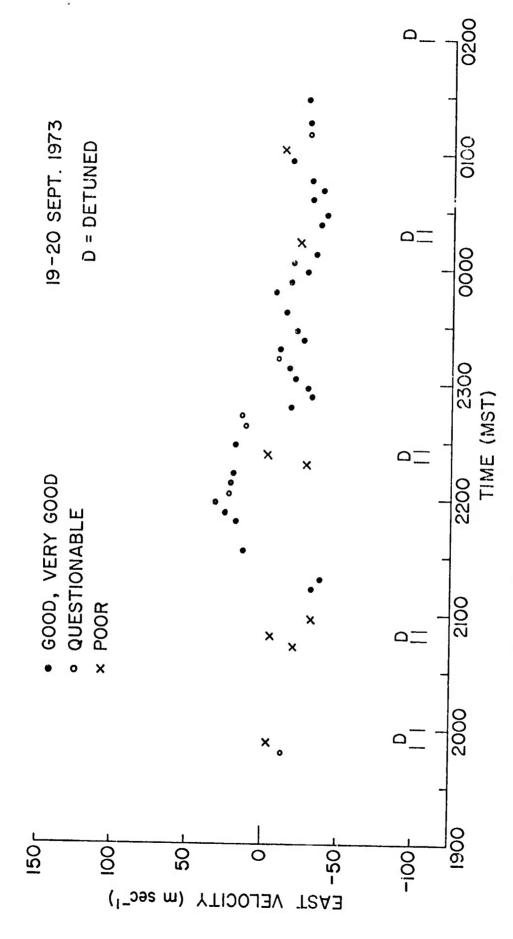
Figure 3.4 Velocities for 18-19 September 1973

Figure 3.5 Velocities for 19-20 September 1975

34
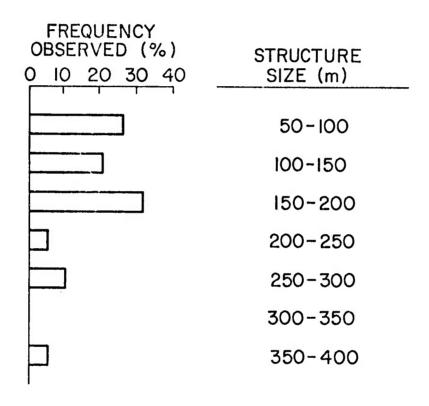
DAYTIME

Figure 3.6 Daytime distribution of structure sizes
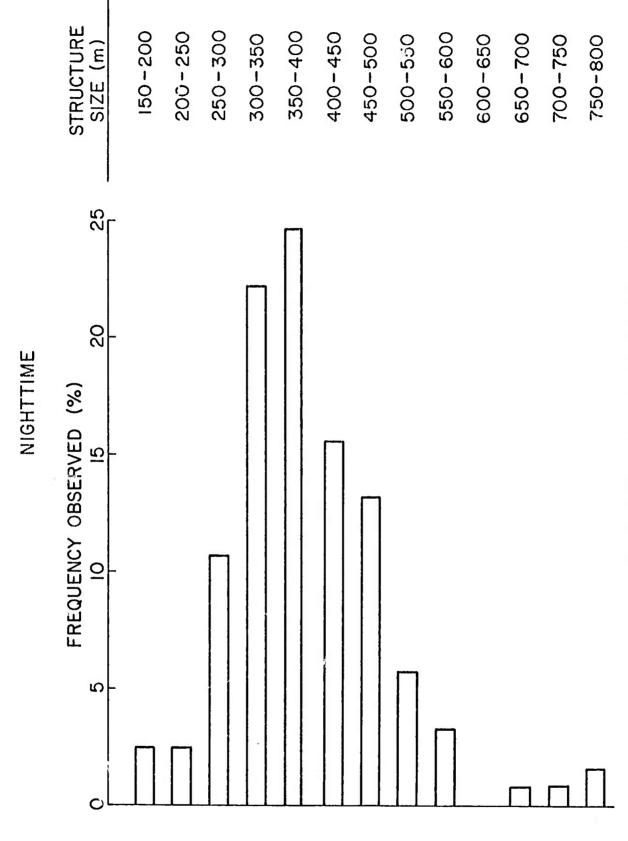
Figure 3.7 Nighttime distribution of structure sizes

```
    DATAFILE, INTERVAL
X91@@@  02

   X91@@@ PART  1
BACKSIDE  1  2      986    976
NO TIME SHIFT       2     1   986    960
       2       3       2
  814    871    910    932    934   910   865   802
       1       3       2
  815    877    923    953    961   945   905   849   779
  1   1    2 MEAN    441. STD DEV    30.SCINT    6.7%
  980   941   881    810
  2   2    2 MEAN    274. STD DEV    21.SCINT    7.6%
  974   929   862    789
  3   3    2 MEAN    366. STD DEV    24.SCINT    6.7%
  977   934   872    802


   X91@@@ PART   2
BACKSIDE  1  2      991    974
NO TIME SHIFT       2     1   991    966
       2       3       2
  865    903    926    937    933   914   884   845
       1       3       2
  868    904    929    943    941   926   900   863
  1 · 1    2 MEAN    459. STD DEV    31.SCINT    6.8%
  980   940   886    826
  2   2    2 MEAN    284. STD DEV    22.SCINT    7.7%
  970   917   849
  3   3    2 MEAN    400. STD DEV    32.SCINT    8.1%
  986   961   927    888   844


   X91@@@ PART   3
BACKSIDE  1  2      989    975
NO TIME SHIFT       2     1   989    959
       2       3       2
  795    869    923    956    964   939   889   817   727
       1       3       2
  764    840    898    938    953   938   897   831   746
  1   1    2 MEAN    446. STD DEV    40.SCINT    8.9%
  978   930   860    773    673
  2   2    2 MEAN    279. STD DEV    28.SCINT   10.2%
  973   918   846    756
  3   3    2 MEAN    420. STD DEV    41.SCINT    9.7%
  976   923   849    762
```

Figure 3.8 Computer geostationary correlation printout

```
   X91000 PART  4
BACKSIDE  1  2      995    979
NO TIME SHIFT       2     1   995    967
        2       3       2
   812    864    915    946    962    961    938    896    837    758
        1       3       2
   789    846    898    935    957    962    946    910    855    780
   1   1    2 MEAN    437. STD DEV     52.SCINT    12.0%
   980    952    900    834    748
   2   2    2 MEAN    279. STD DEV     37.SCINT    13.3%
   971    946    890    825    740
   3   3    2 MEAN    445. STD DEV     64.SCINT    14.4%
   983    953    906    846    775

   X91000 PART  5
BACKSIDE  1  2      995    951
NO TIME SHIFT       2     1   995    937
        2       3       2
   758    841    920    964    963    924    842    734
        1       3       2
   738    829    911    961    968    936    861    757    626
   1   1    2 MEAN    439. STD DEV     38.SCINT    8.7%
   953    899    807    687
   2   2    2 MEAN    285. STD DEV     29.SCINT    10.1%
   937    886    795    673
   3   3    2 MEAN    457. STD DEV     52.SCINT    11.4%
   965    908    815    695

   X91000 PART  6
BACKSIDE  1  2      993    933
NO TIME SHIFT       2     1   993    930
        2       3       2
   810    871    933    955    927    866    764
        1       3       2
   803    871    932    957    934    875    776
   1   1    2 MEAN    453. STD DEV     32.SCINT    7.0%
   946    894    808    706
   2   2    2 MEAN    293. STD DEV     23.SCINT    7.9%
   921    872    781
   3   3    2 MEAN    471. STD DEV     39.SCINT    8.3%
   952    886    785
```

Figure 3.9 Computer geostationary correlation printout

Immediately under the section "X91@@@ PART 1" the line indicates the backside of the correlation of antennas 1 and 2 was found since the correlation dropped from 0.986 at T = 0 to 0.976 at T = 2. The next line indicates no further time shifts were calculated since the correlation of antenna 2 to 1 dropped from 0.986 at T = 0 to 0.960 at T = 2. Therefore the peak of the cross correlation curve between these two antennas is at T = 0. The next line indicates that the correlation of channels 2 and 3 was calculated by time shift increments of two, and the correlations starting at T = 0 are given on the following line, e.g., 0.814 at T = 0 and 0.802 at T = 14. The next pair of lines are for channels 1 and 3. Note that the correlations for channels 2 and 3, as well as 1 and 3 rise to a peak at some time shift and then fall. The last six lines under "X91@@@ PART 1" are the auto correlations of the three channels. The first line of the auto-correlation section indicates that channel 1 was correlated with channel 1 (auto correlated) by time shift increments of two. The mean, standard deviation, and scintillation of channel 1 are given for checking the quality of the data. The scintillation printed here has a different definition than one used elsewhere and cannot be directly compared. Similarly, results are given for channels 2 and 3.

The program used for this processing is normally set to calculate correlations for a number of data files. More details about the data files can be found in the appendix of this report. Normally, an entire day (8 hours) of data takes about 5 hours to process.

3.4 Orbital observations

As the LOS between the receiving station and the orbiting satellite sweeps through the disturbed region, the orientation and size of the disturbances may be deduced. In the model we have been using, the disturbances are field aligned and quite long with respect to the axial dimensions. These field-aligned irregularities throw long thin "shadows" which have a certain orientation and

39

velocity. Knowing the parameters of both the satellite orbit and the magnetic field lines in the heated region, this orientation and velocity may be calculated. The results may be compared with the measured value of irregularity orientation and speed.

An orbital pass was recorded on 20 September 1973 from Hillsdale, Wyoming in which this calculation may be performed. During this satellite pass, the signal was received on three antennas in a right triangular configuration as described earlier in this report. There was an east-west pair of antennas and a north-south pair. Figure 3.10 shows the auto correlation of the amplitude of the satellite at one of the antennas at 05:55:30 GMT for that pass. The cross correlation of the amplitudes received at the north and south antennas is also shown. The cross correlation of the signals from the east and west antennas was also computed, but is not shown here. These cross correlations can be used to calculate N-S and E-W time shifts, and the results used to determine the orientation and velocity of the pattern on the ground (Bowhill, et al., 1972). The results are tabulated below.

Hillsdale, Wyo. 20 September 1973 05:55:30 GMT

Time shifts	22 ms north to south 16 ms west to east
Antenna spacing	N-S - 66.38 m E-W - 63.74 m
Apparent velocities	3.74 km/s eastward 3.02 km/s southward
Total velocity	2.07 km/s at 141° bearing (i.e., east of north)

These results may be compared with the calculated speed and direction based on the magnetic field alignment model. At 05:55:30 GMT, the satellite had a range of 1100 km, a bearing of 158°, and an elevation angle of 76°. It was moving northward with a velocity of 7.25 km/sec. Using calculations similar to those shown by Bowhill and Ward (1973), it may be shown that the magnetic
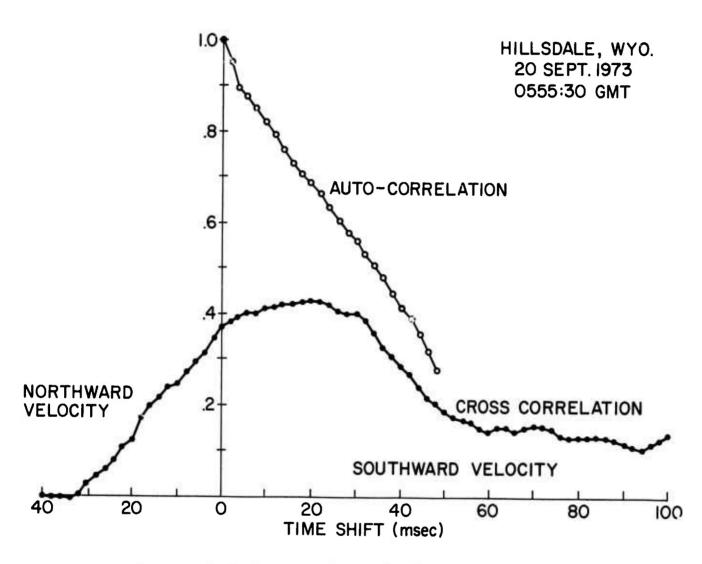
Figure 3.10   Orbital correlation for Hillsdale, Wyo. 20 September 1973

field-aligned irregularities (dip = 68.2°) produce long, thin shadows whose alignment is 50.4° east of north. Due to the satellite velocity, these patterns move on a bearing normal to their alignment (bearing = 140.4°) with a speed of 1.99 km/sec. The results of these two calculations are summarized below.

	"Shadow" Velocity	
	Speed	Bearing
Calculated	1.99 km/s	140.4°
Measured	2.07 km/s	141°

The very good agreement in these paramters tends to further confirm the conclusion that the ionospheric ASF irregularities are field aligned.

The structure size may next be determined from the autocorrelation curve. The 1/e point for the autocorrelation curve is found at 44 ms. Multiplying this by 2 km/sec gives a structure size of 88 meters for the pattern on the ground (shadow). The ratio of the distance to the satellite compared with the distance to the heated region is used to compute the ratio of the structure size on the ground to the structure size in the heated region. The 1/e structure size in the heated region was thus computed to be 64.2 m. This may be compared to a range of values for structure size from about 60 m to about 250 m seen on 8 September 1972 from Kimball, Nebraska (Bowhill and Ward, 1973b).

3.5 Mathematical model

The model which we have been using to describe the scintillation effects (Bowhill, et al., 1972, pages 74 and 75, and Briggs and Parkin, 1963) can be used to predict the relationship between the scintillation index and the angle between the magnetic field and the LOS to the satellite.

From the standard Briggs and Parkin theory, the scintillation index S is directly proportional to the RMS phase fluctuation γ. The value of γ may be found from

$$\gamma^2 = \frac{\pi^{5/2}}{\lambda^2} \left(\frac{foF2}{f}\right)^4 D \left(\frac{\Delta N}{N}\right)^2 \sec (i) \cdot$$

$$\csc \psi \cdot \int_0^{h_s} \exp\left[\frac{-(x-x_0)^2}{R^2}\right] \exp\left[\frac{-(h-h_m)^2}{H^2}\right] dh$$

where the terms are defined in Figure 3.11.
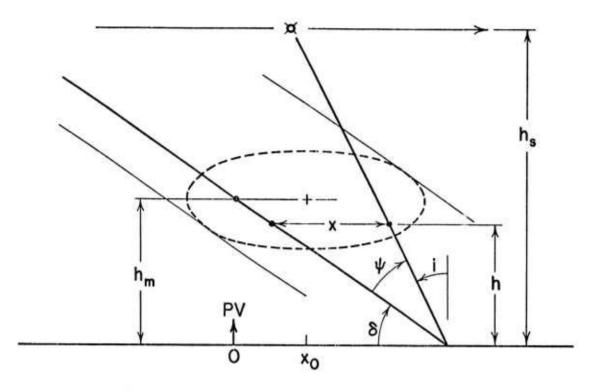
We are using a field-aligned Gaussian distribution shifted x_0 km north of overhead Platteville. The e-folding vertical distance is H, and the e-folding horizontal distance is R. As can be seen, we are integrating along the LOS from the observer to the satellite. If this integration is carried out, we find

$$\gamma^2 \propto \frac{RH \csc \psi \csc (\delta + \psi)}{\sqrt{R^2 + H^2 u^2}} \exp\left\{\frac{-(x_0 - h_m u)^2}{(H^2 u^2 + R^2)}\right\}$$

where $u = \tan \psi (1 + \cot \delta \cot (\delta + \psi))$.

A computer program has been written to evaluate this function. The results may be compared with actual data by plotting scintillation index versus the angle to the magnetic field for both the experimental and the theoretical data. Values of horizontal and vertical e-folding distances as well as horizontal displacements north or south of Platteville may be varied to find a "best fit" to the available data.

Examples of plots of scintillation index versus magnetic field for several satellite passes are shown in Figures 3.12 through 3.15. These are followed by theoretical curves of normalized γ (directly proportional to scintillation index) as a function of ψ (angle between LOS and magnetic field) for various parameters. Figure 3.16 shows how the curves differ for various values of the height of maximum heating. Figure 3.17 shows a family of curves for various e-folding

δ = Local dip angle (= 68.2°)

h_s = Height of satellite

h_m = Height of maximum of heated region

x_0 = Distance (north) of overhead Platteville (PV) of maximum of heated region

i = Incidence angle of satellite

h = Height of point of integration

x = Distance (horizontal) between point of integration and field line through observer

ψ = Angle between LOS to satellite and magnetic field

Figure 3.11 Geometry for Briggs and Parkin theory application
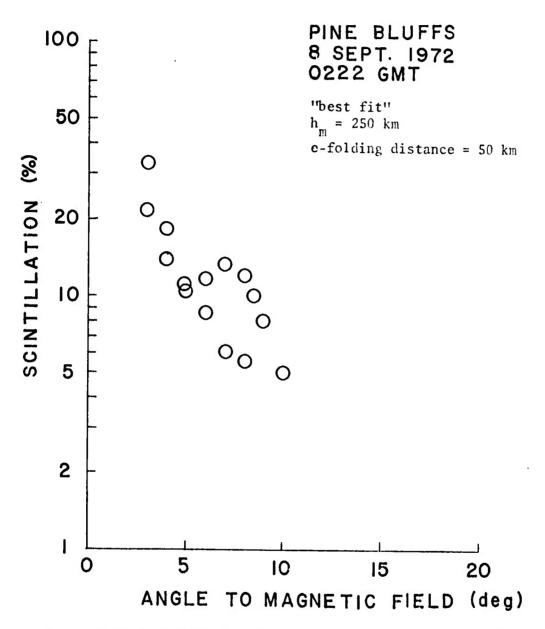
Figure 3.12 Scintillation index versus angle to magnetic field for Pine Bluffs 8 September 1972 02:22 GMT
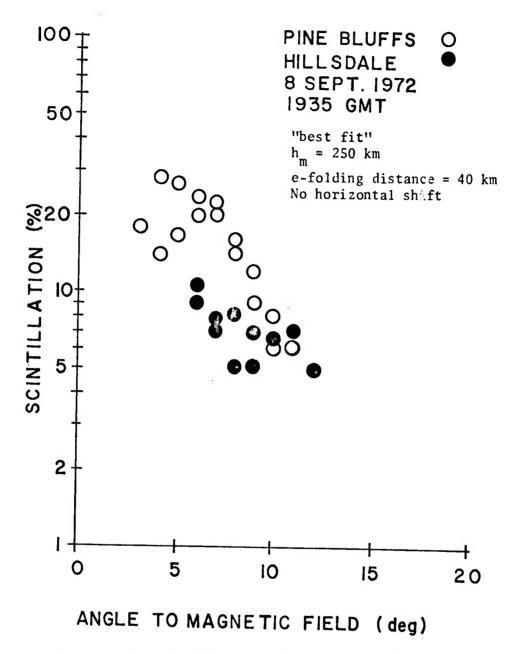
Figure 3.13   Scintillation index versus angle to magnetic field for Hillsdale 8 September 1972 19:35 GMT
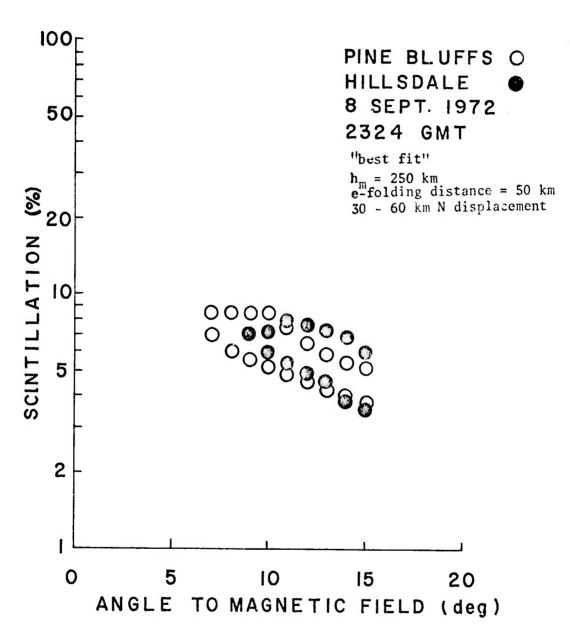
Figure 3.14 Scintillation index versus angle to magnetic field
for Hillsdale 8 September 1972 23:24 GMT
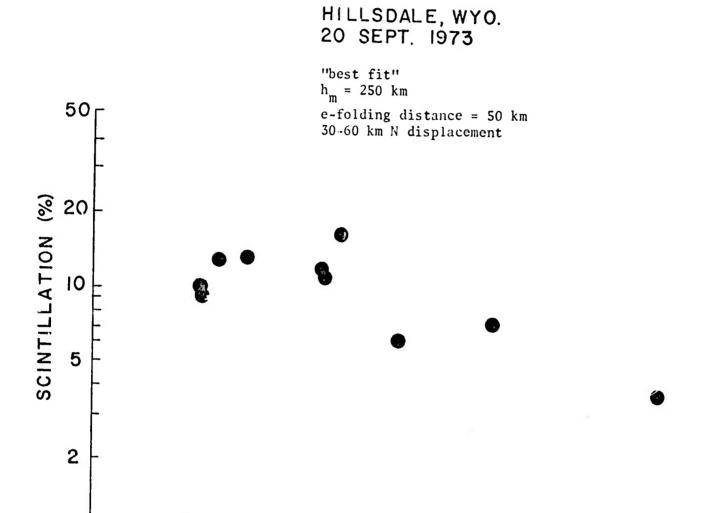
Figure 3.15 Scintillation index versus angle to magnetic field for
Hillsdale 20 September 1973
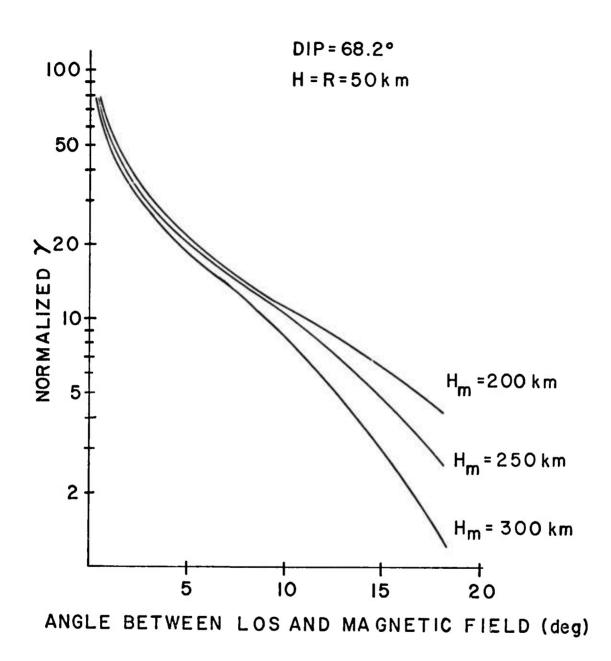
Figure 3.16   RMS phase fluctuation as function of angle to
magnetic field and height of heating

49
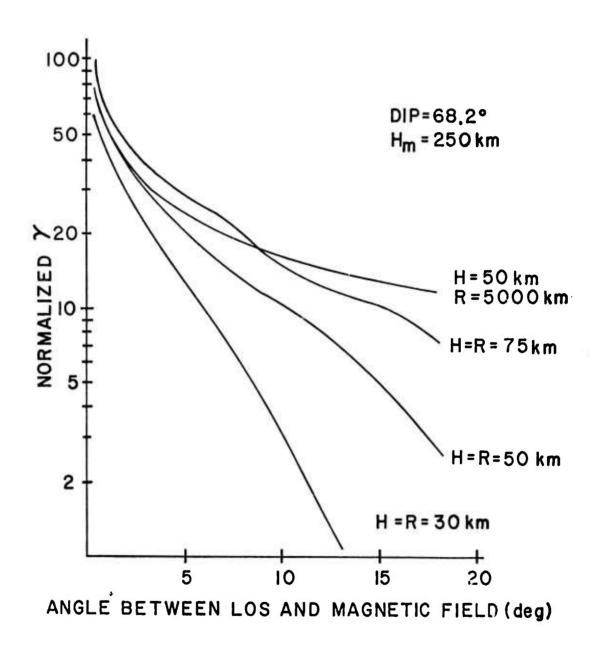
Figure 3.17   RMS phase fluctuation as function of angle to
magnetic field and e-folding distances

distances. The curve for H = 50 km, R = 5000 km shows the shape of the curve if the horizontal extent of the region were essentially infinite. In this case, the variation in γ due only to the change in ψ is displayed. Figure 3.18 gives the variation in γ versus ψ as the heated region is displaced to the north of Platteville.

The parameters of the heated region may be estimated by finding a "best fit" curve for the data. Shown on each experimental data plot are the values of the parameters which give a fit to the displayed data. In general, an e-folding distance of 50 km and a 30 km north displacement seem to fit the data well for h_m = 250 km.
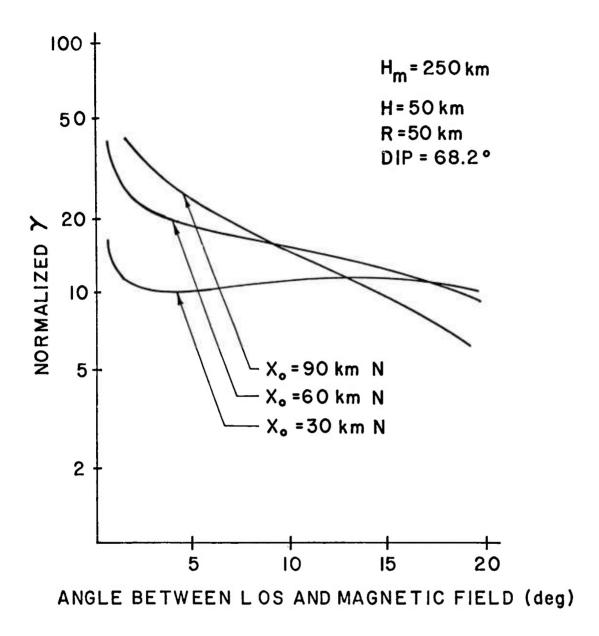
Figure 3.18 RMS phase fluctuation as function of angle to
magnetic field and displacement of the center
of the heated region

4. MAPPING AND YIELD

4.1 Introduction

A number of both orbital and geostationary transmission experiments have been performed in which the transmitter yield as well as the morphology of the heated region may be deduced. The orbital satellite station performs a rapid scan through the heated region, allowing the horizontal and vertical extent to be studied. The geostationary station, on the other hand, observes the variation of the region during power variations, and gives insight into the relationship between power and scintillation index (yield) for the stationary LOS.

4.2 Analysis of geostationary yield

The yield of the Platteville transmitter with respect to scintillation index was studied using the geostationary experiment.. The scintillation index S is calculated from the amplitude A by the expression (Bowhill, et al., 1972)

$$<A^2>/<A>^2 = S^2 + 1$$

4.2.1 Ambient geostationary

In order to find the baseline scintillation, the geostationary experiment was operated on 24 September 1973 when no heater was present. The scintillation index is displayed in Figures 4.1 and 4.2. The baseline scintillation index is about 1.5% with noise peaks occasionally higher. The heater is turned on near the end of the period in Figure 4.2 with small effects seen until the power is at -3 dB.

Since the time response of the scintillation index to variations in power is on the order of a minute or so, the Type 1 power stepping experiment in which the power was varied in steps for 10-minute intervals was chosen as the yield diagnostic. The most reliable Type 1 experiment with respect to heater operation, power calibration, and geostationary data reliability was performed on 20 September

53
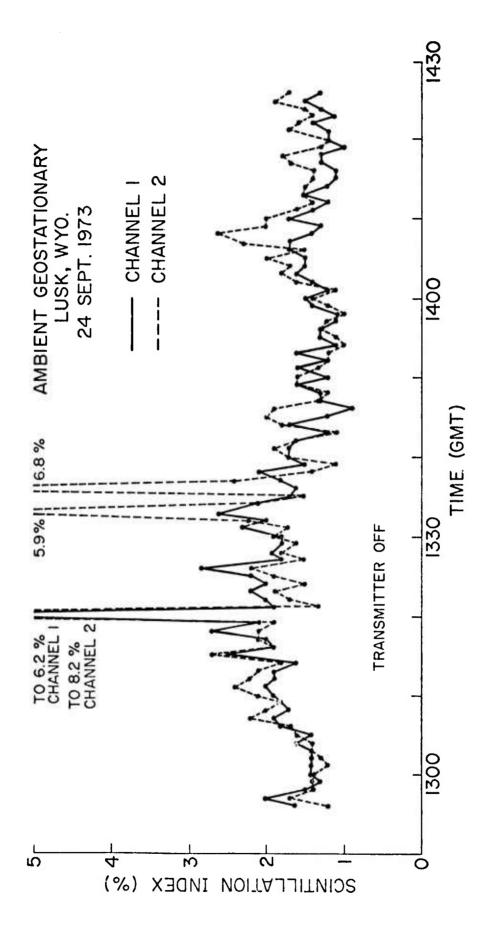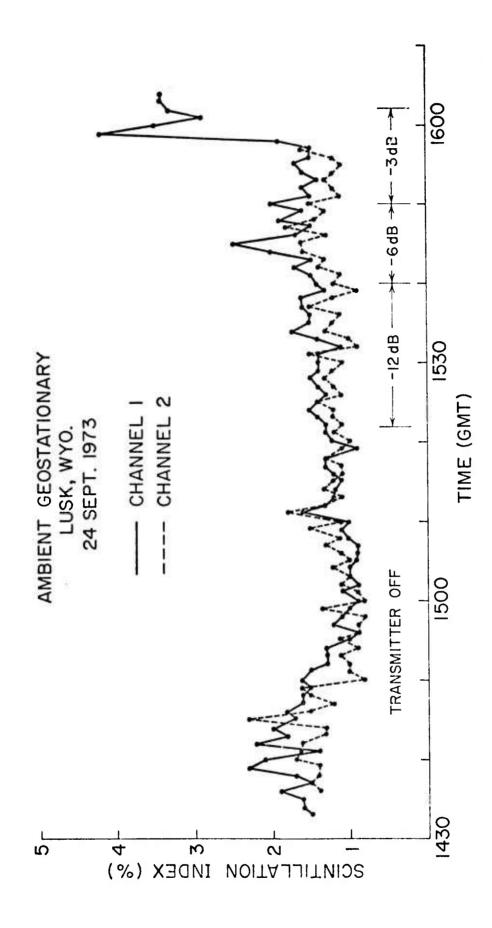
Figure 4.1 Ambient geostationary scintillation index 24 September 1973, Part 1

54

Figure 4.2 Ambient geostationary scintillation index 24 September 1973, Part 2

1973 from 2100 to 2200 MST. These data are displayed in Figure 4.3. As can be seen in this figure, the ratio of f_H to foF2 was held fairly constant as the power was increased. The increase in scintillation index is clearly seen.

4.2.2 Analysis

In an attempt to accurately determine the relationship between the scintillation index and the transmitter power, the data shown in Table 4.1 were tabulated. The value of the mean scintillation index was determined by omitting the first minute from each group and averaging the remaining data. The power was determined from the Platteville transmitter logs. These data were next plotted on log-log paper to determine the quantity x in the relationship $S \propto P^x$. The results are shown in Figure 4.4. As can be seen, data points 2 through 5 lie approximately on a line of slope x = 1.0. Data point 1 with power = 0 cannot be shown on a logarithmic scale. Point #6 for the highest value of power (0.970 MW) seems to exhibit a saturation effect, while point #7 is derived from a short group of data following the 0.970 MW sequence. It should be pointed out that this yield result ($S \propto P^1$) differs from an earlier Prairie Smoke result showing $S \propto P^{1/2}$ (Walton, et al., 1973). The earlier data however were based on a scatter plot of data collected over a long period of time rather than a power-stepping experiment as described here. Also, the earlier power calibrations were less reliable than the power data presented here.

4.3 The Redbird experiment

On the night of 18 September 1973 (19 September GMT date), the geostationary satellite ATS-6 was received by two stations. One station was the Lusk receiving station described earlier in this report. The other receiving station used a single receiver mounted in the mobile Winnebago shell. This receiving station was located 57.4 km north of the Lusk station at Redbird, Wyoming. The LOS from Lusk to ATS-5 passed over Platteville at 275 km height, while the LOS from

Table 4.1

Tabulation of power and scintillation index for the
September 20, 1973 Type 1 Yield Experiment

Point	Time GMT	Mean scint. index Ch 1	Ch 3	Power (MW)
1	0400-0410	1.75	1.77	Off
2	0410-0420	1.51	1.56	0.188
3	0420-0430	2.14	3.00	0.299
4	0430-0440	4.36	3.75	0.390
5	0440-0453	4.11	5.33	0.598
6	0453-0459	4.36	3.92	0.970
7	0459-0502	7.50	10.05	0.270
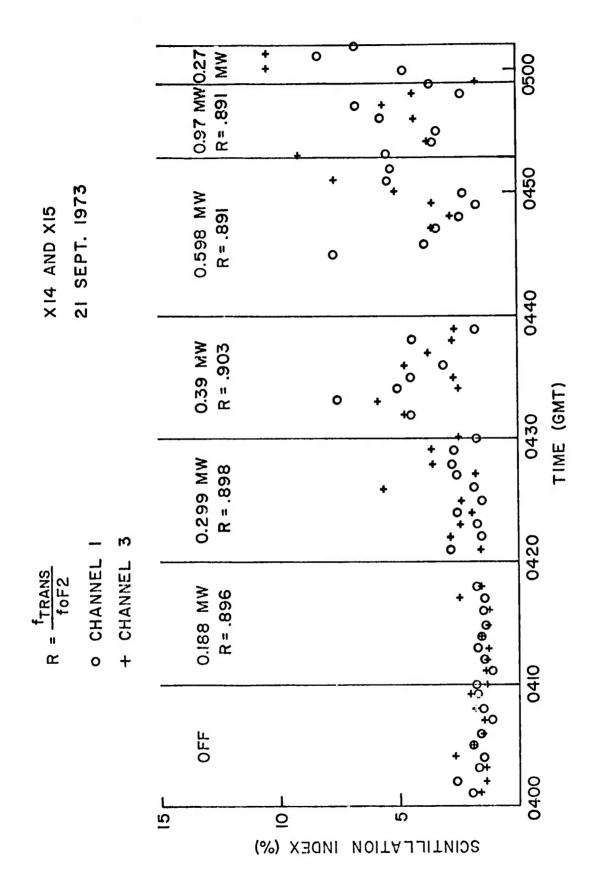
Figure 4.3 Geostationary scintillation index during power stepping 21 Sept. 1973

58
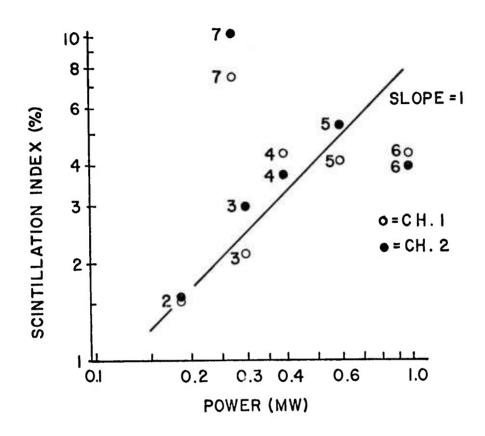
Figure 4.4   Scintillation index versus power

Redbird passed over Platteville at 328 km (a difference of 53 km). The elevation angle of the geostationary satellite was 42.5 deg.

The scintillation index computed during the Redbird geostationary experiment is shown in Figures 4.5, 4.6, and 4.7. These figures show the scintillation index computed from the signal received at both Lusk, Wyoming, and Redbird, Wyoming from 0600 to 1020 GMT on 19 September 1973. The scintillation index of the signal received at the Lusk site was computed from data stored on digital magnetic tape in the same manner as described earlier in this report. The scintillation index of the signal received at Redbird was computed by detecting, filtering and digitizing the analog tape records of the signal which were made during this experiment.

The power data shown in Figures 4.5, 4.6, and 4.7 were prepared from the "log of measured transmitter output" supplied by SRI for these times. The value of foF2 = 3.03 MHz was reported to be constant over the entire period. The transmitter frequency was also held constant during this time at 2.8 MHz. This gives a ratio f_H/foF2 = 0.924 for the entire period.

The scintillation data, in spite of the stability of the ionosphere, are quite variable with time. It can be seen that extended periods of reduced power (10 minutes or more) correspond to periods of reduced scintillation index. On the other hand, extended periods of constant full power operation (Figure 4.7) yield large variations in the scintillation of the signal received at both Lusk and Redbird. Detailed comparison of the Redbird versus the Lusk scintillation index shows a great deal of short-term variation. There is somewhat greater long-term (15 minutes or more) similarity however. This implies that there does exist a certain amount of correlation between the region probed from the Lusk site and that probed from the Redbird site.

It is clear that some further analysis of these data can be performed. A more accurate measure of the correlation between the Lusk and the Redbird data

60
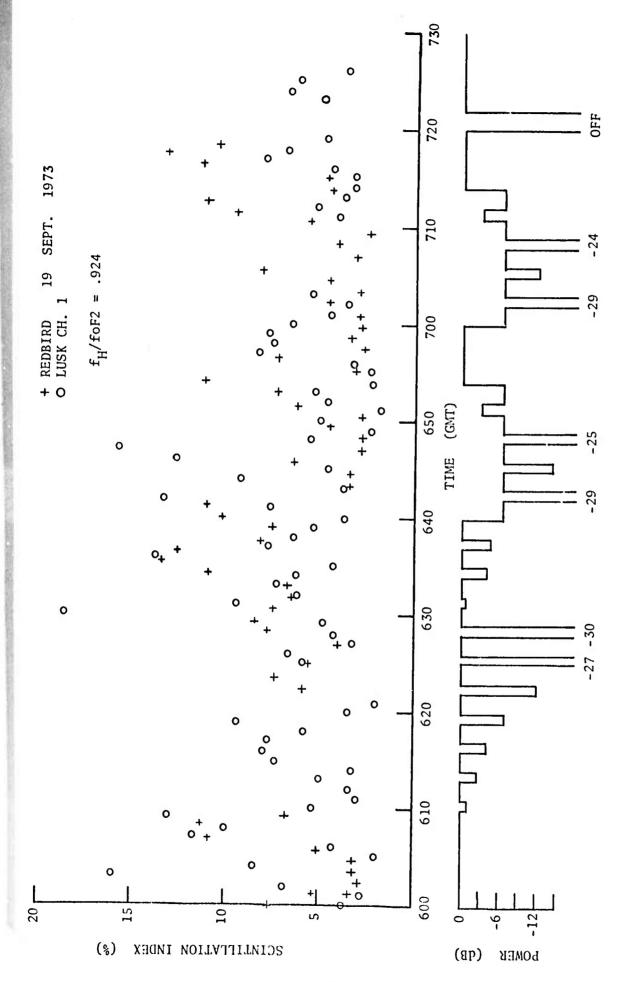
Figure 4.5 Scintillation index for Redbird and Lusk 19 Sept. 1973, 0600-0730 GMT

61
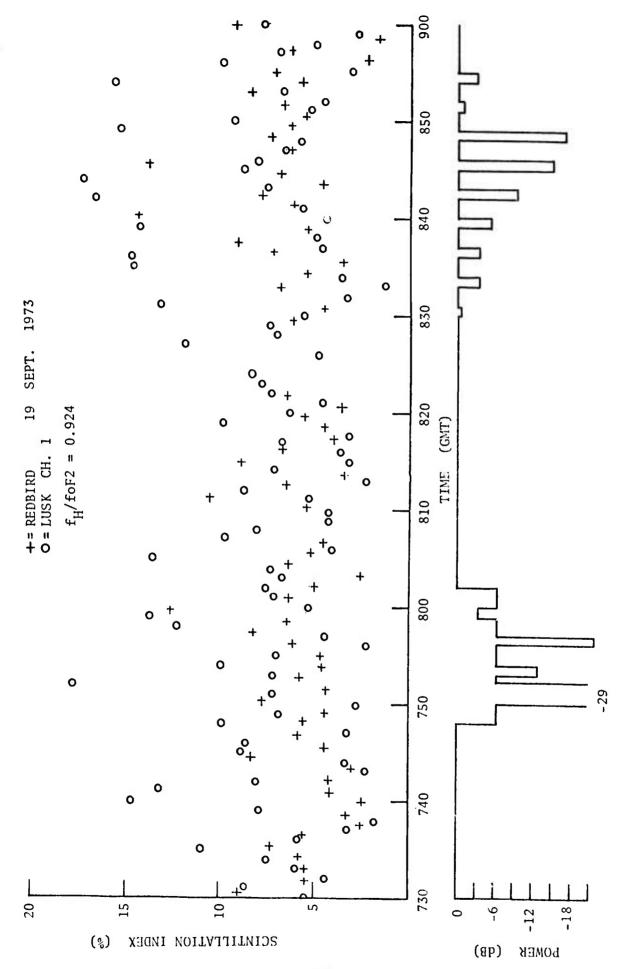
Figure 4.6 Scintillation index for Redbird and Lusk 19 Sept. 1973, 0730-0900 GMT
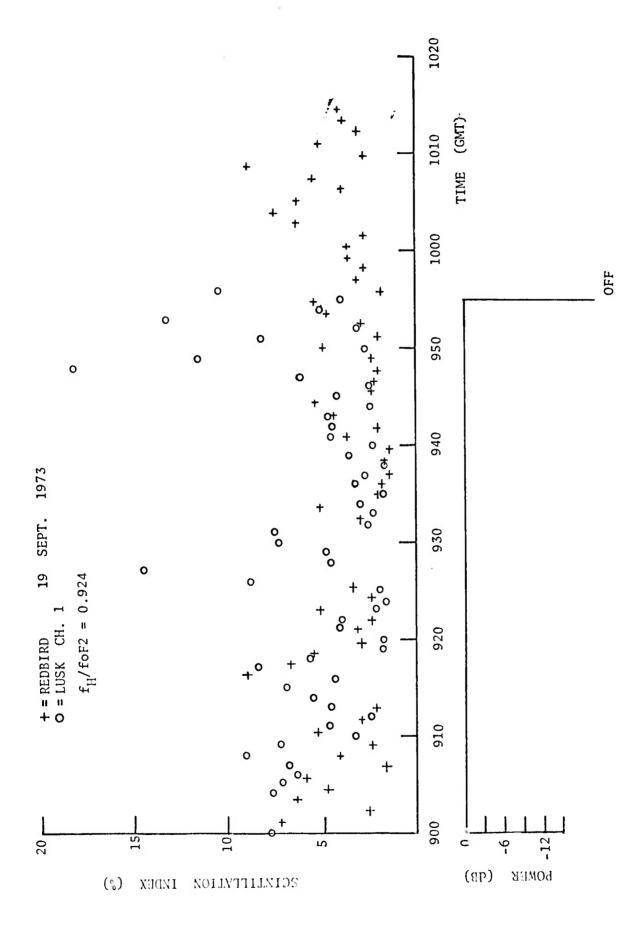
Figure 4.7 Scintillation index for Redbird and Lusk 19 Sept. 1973, 0900-1020 GMT

has been computed. The scintillation data were entered into a computer, and the auto- and cross correlations were computed. Figure 4.8 is the auto correlation of the scintillation index values for both the Lusk and the Redbird receiving sites. Note that there is evidence of a 6 minute (or so) periodic structure in both sets of data. The periodic structure seems much more predominant in the scintillation data computed at Lusk than at Redbird. These data were next cross correlated, and the results are shown in Figure 4.9. Once again, 6-minute periodic effects may be seen, although the magnitude of the cross correlation is rather small. There is a time (or phase) shift of these periodic effects of about -1 minute. This implies a resultant velocity of 900 m/s southward for these periodic effects. These results are consistent with an actual velocity which is largely east-west and considerably smaller than this resultant north-south value.

4.4 Extended scintillation studies

For the night of 17 September 1973, a continuous record of the scintillation index as a function of time has been computed. This record begins at 23:15 MST September 17, 1973 and ends at 06:45 MST September 18, 1973. A great deal of simultaneous other data have been provided by SRI, and may be compared to the scintillation index data. Figures 4.10 through 4.14 show plots of the various data provided Aeronomy Corporation. The values of the scintillation index were calculated by the scintillation formula described earlier in this report. The other data displayed in these figures were provided by SRI. The radar cross sections were obtained from the SRI radar facility near White Sands, New Mexico. The transmitter power and the values of foF2 were taken from the Platteville transmitter logs. Also available were ionograms taken at Boulder, Colorado during the experiment. These data have all been incorporated into Figures 4.10 through 4.14.

Several interesting observations may be made concerning these data. First,

64
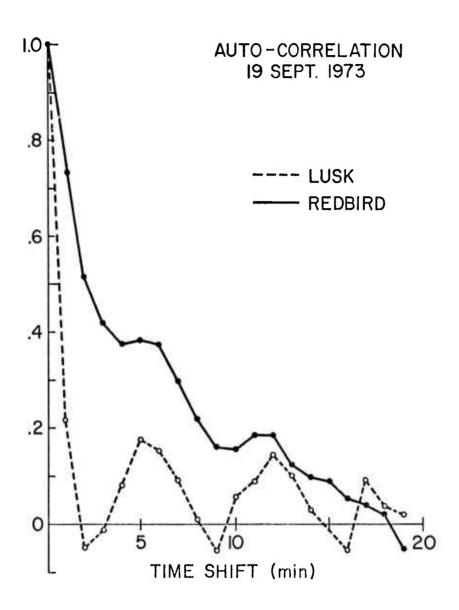
Figure 4.8 Autocorrelation of Lusk and Redbird data
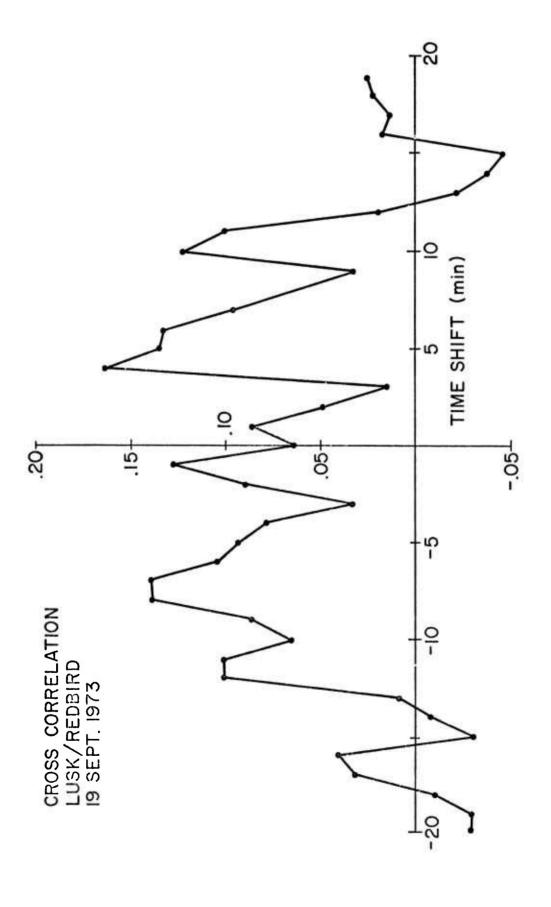
Figure 4.9 Cross correlation of Lusk-Redbird data
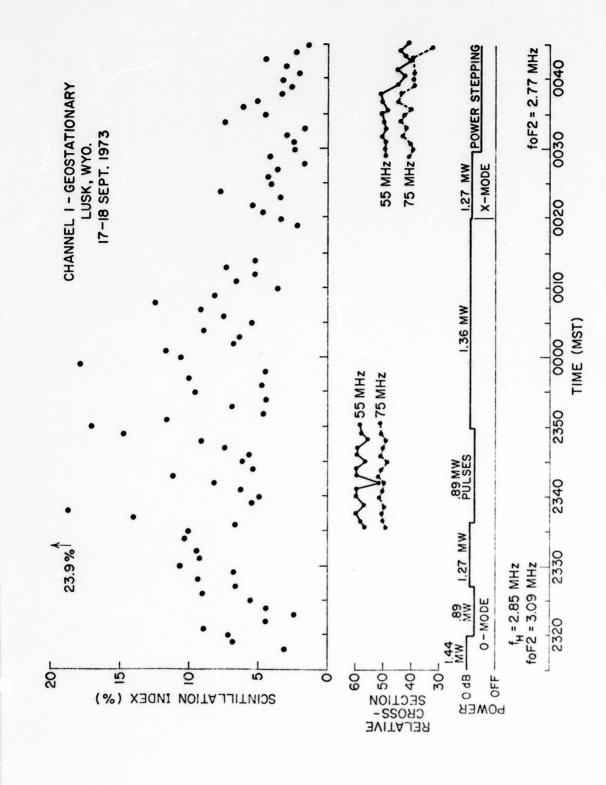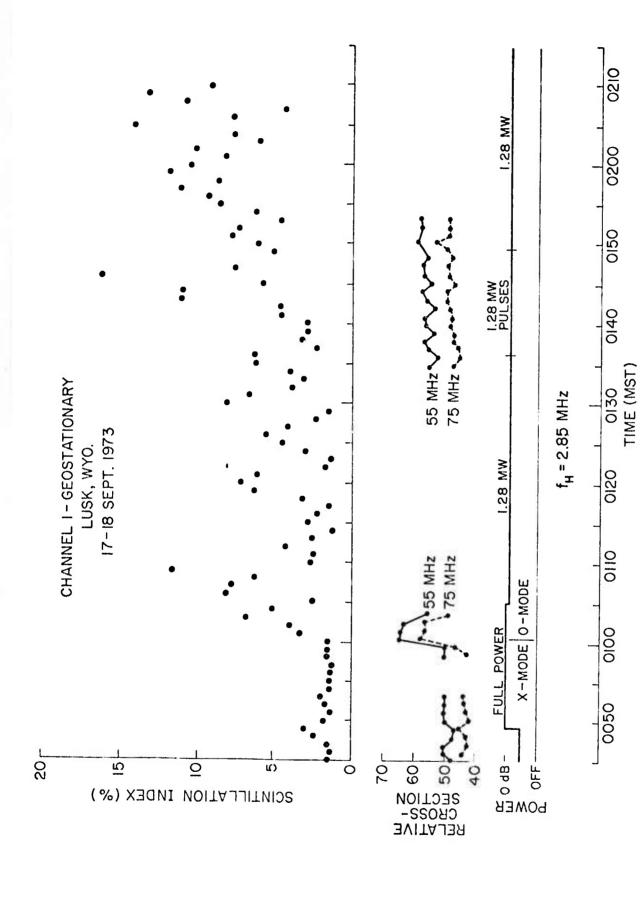
Figure 4.10 Scintillation index Lusk 17-18 Sept. 1973, 2315-0045 MST

67

Figure 4.11 Scintillation index Lusk 17-18 Sept. 1973, 0045-0210 MST

68
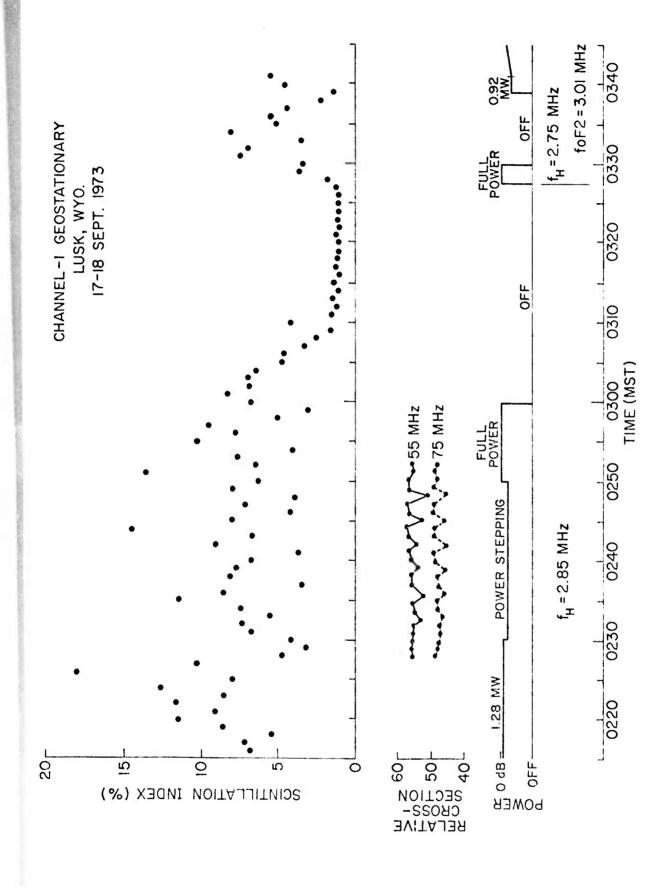
Figure 4.12 Scintillation index Lusk 17-18 Sept. 1973, 0215-0345 MST
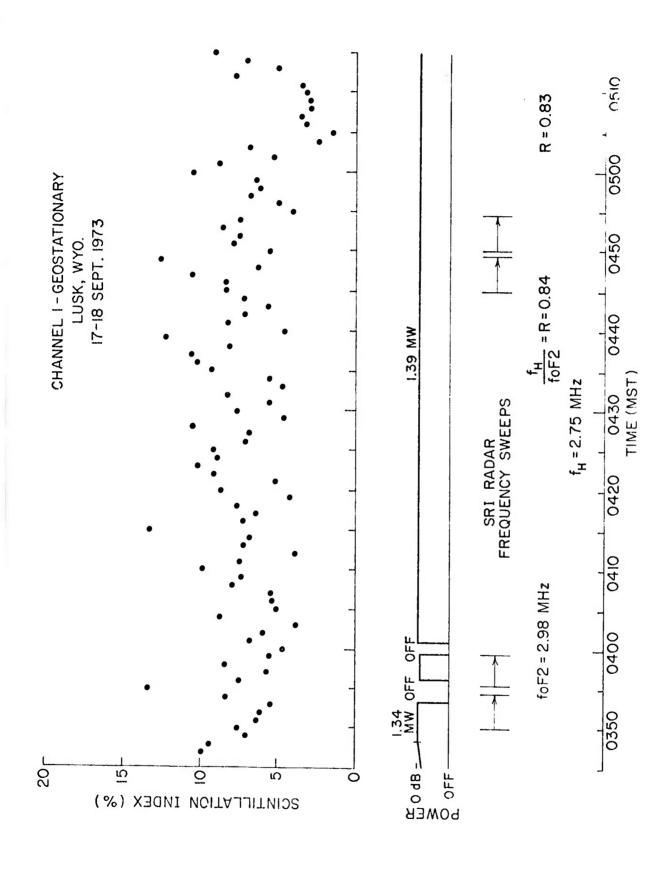
Figure 4.13 Scintillation index Lusk 17-18 Sept. 1973, 0345-0515 MST
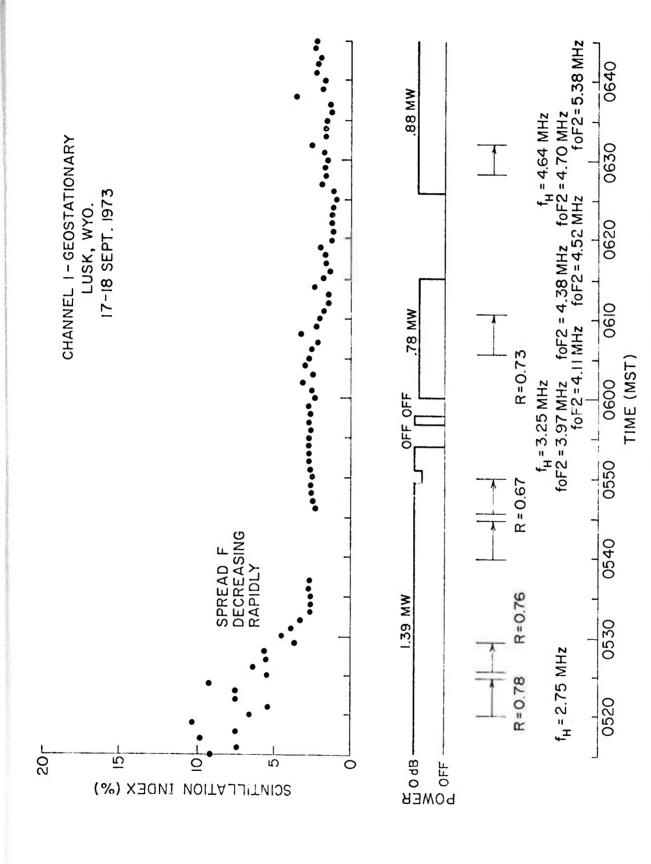
Figure 4.14 Scintillation index Lusk 17-18 Sept. 1973, 0515-0645 MST

71

the data points shown in the scintillation index section of these figures each requires processing of 60 seconds length of geostationary satellite amplitude data. This means that the sections containing pulses and power steps cannot be used on a one-to-one basis since the pulse and power parameters are being changed as rapidly as once per minute. The relative cross section data available during these special times gives a good indication of the power variations, but the ionospheric response with respect to the production of scintillations is too slow to respond to the rapid variations.

The effect of transmitter variations with time scales of 5 minutes or more may be more easily seen in the scintillation index plot. The transmitter was switched to X-mode heating from 00:20 MST to 01:00 MST, for example. When the switch was made from 0-mode to X-mode heating at 00:20 MST, the general level of scintillation can be seen to have been reduced from about 7% to about 4%. The value of f_H, foF2, and heater power (P_H) all remain rather constant during the change. The switch back to 0-mode heating at 01:00 MST is more dramatic. As can be seen, the values of f_H, foF2, and P_H are all constant as the switch is made from X-mode to 0-mode heating. The scintillation increases rapidly from about 2% (equal to the ambient level) to an average of 6% or more. A rapid increase in the relative cross section may also be seen at this point. The time response of the scintillation index following a transmitter switch-off may be seen at 03:00 MST.

This switch-off was preceded by 10 minutes of full power cw. At the time of the switch-off, the scintillation index has reached about 8%. This index drops to about 2% in 9 minutes or so. This 9-minute decay rate is larger than the typical daytime value of about 1-5 minutes.

This off period was followed by 3 minutes of full power operation from 3:27 until 3:30 MST. As can be seen, this 3-minute "burst" of power causes a rapid onset in the scintillation index (rise from 2% to 8% in about 3 minutes)

72

which seems to overshoot a bit before decaying in the previously observed time of about 9 minutes.

A final item on these figures is of particular interest. The period from 05:15 MST till 05:35 MST shows a marked decrease in the scintillation index, the radar cross section, and the amount of observable artificial spread F (ASF). During this time, the value of foF2 was increasing rapidly while the value of f_H = 2.75 MHz and the transmitter power of 1.35 MW was held constant. The speed with which the scintillations drop from about 9% down to about 3% is comparable to the scintillation decay time discussed earlier of 9 minutes. During this 9-minute period, the ASF can be seen to decay from a condition of very severe to an F-region trace that seems nearly normal for an undisturbed ionospheric F region. The radar cross section data (available as frequency sweeps during the times marked "S" on the figures) was also observed to drop rapidly. Figure 4.15 is a plot showing the relationship between the radar cross section (at 55 MHz) and the average scintillation index for various times during this drop-out as well as an extra "fill the gap" point taken at 00:35 MST. As can be seen, there is a nearly linear relationship between cross section and average scintillation index.

4.5 Orbital morphology

A number of observations of the scintillation of orbital satellite signals after propagation through the heated region have been made. Most of the data and interpretations are available in the past series of Prairie Smoke reports. In general, the overall heated region is found to be a field-aligned Gaussian ellipsoid centered at the F-region maximum. It has an e-folding radius of about 50 km, and its center is typically located about 30 km north of the Platteville transmitter. There is a great deal of variation about this typical case, however. The orbital experiment will often show a patchiness or perhaps even a "hole" in the center (burn through) of the cloud (resulting in a doughnut-shaped cloud) over Platteville.

73
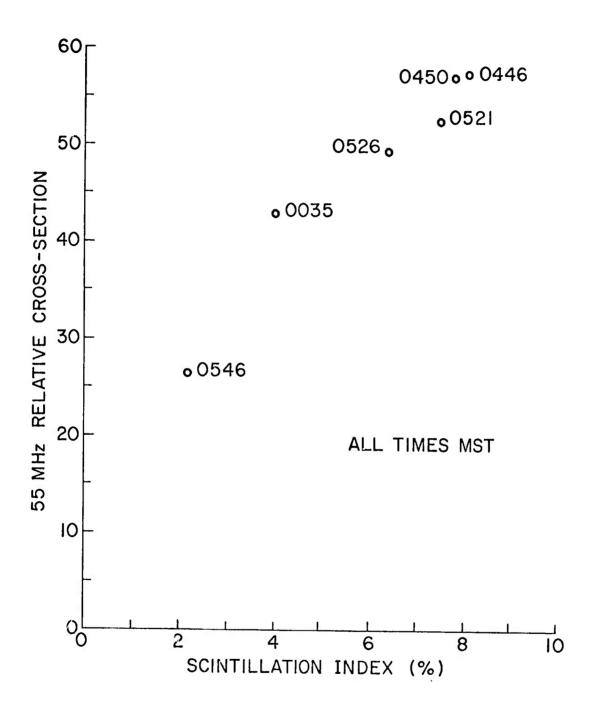
Figure 4.15   Relation between scintillation index and
relative cross section 18 September 1974

Of particular interest is the scintillation data from the Hillsdale site for 20 September 1974. In these data, E_s-region as well as F-region effects are evident. The ionogram for that experiment (Figure 4.16 shows a very strong E_s layer (at 100 km) as well as the F-region traces. The scintillation index data seen in Figure 4.17 may thus be interpreted with respect to both E_s and F-region effects. The peak in the scintillation index curve (Figure 4.17) from 0555 to 0556 GMT can be matched with an F-region cylinder 50 km in radius, 30 km north of Platteville (Figure 4.18). The peak in Figure 4.17 from 05:53:45 to 05:54:30 GMT corresponds to an E_s cylinder with 35 km radius shifted 40 km north of Platteville (Figure 4.19). The proper cylinder was determined by adjusting the radius and distance north until the cylinder model showed that the LOS passed above and below 100 km corresponding to the start and stop of scintillations. The E_s-region scintillations are found to exist even though the heater transmitter was operated on a frequency chose to enhance the F-region effects. Also, the cylinder model which matches the observed E-region scintillation data was smaller in radius (35 km) than the F-region cylinder (50 km). Both cylinders were displaced north of overhead Platteville (40 km north for the E_s region and 30 km north for the F region). Finally, it should be pointed out that since this is the first available crossfield data, this is the first time that the agreement with the cylinder model for such a configuration could be confirmed. A height range from 220 km to 340 km was determined for the disturbed region on 28 September 1973, when the true height of reflection of the heater signal was reported as 232 km.

A further consequence of the field-aligned ellipsoid model under study here is the possibility of multipath. As the orbital satellite nears an up-field position, the possibility of reflection of the signal from the irregularities increases. It may be possible for the receiving station to receive this reflected signal as well as the direct signal for a short time. Characteristic

75

05:53:59 GMT
20 SEPTEMBER, 1973

foF2 = 3.62 MHZ
f_H = 2.85 MHZ at 1.44 MW

FREQUENCY (MHZ)

HEIGHT (KM)
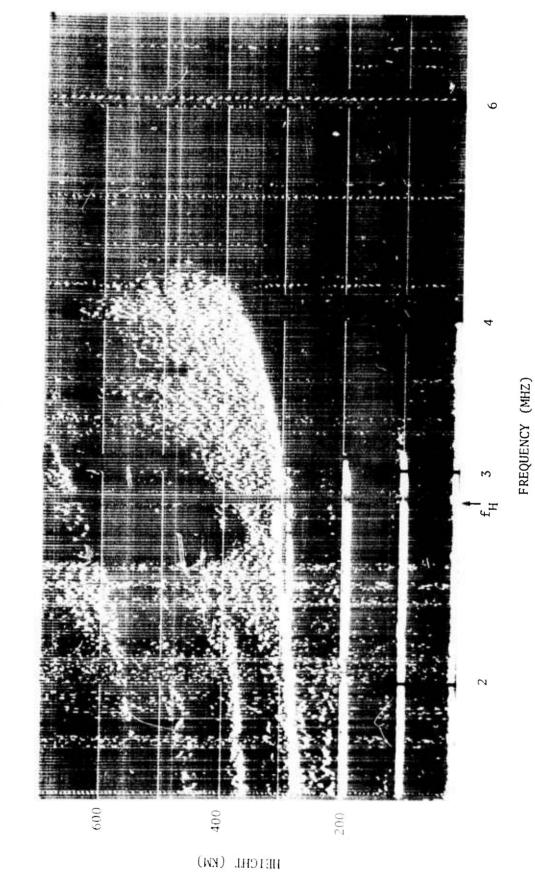
Figure 4.16   VI ionogram at Erie, Co. 20 Sept. 1973, 05:55:59 GMT
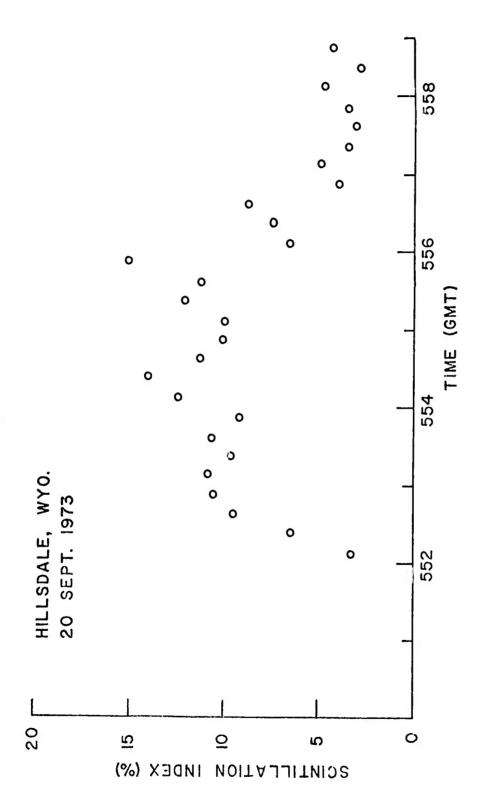
Figure 4.17 Scintillation index for Hillsdale, Wyo. pass 20 Sept. 1973
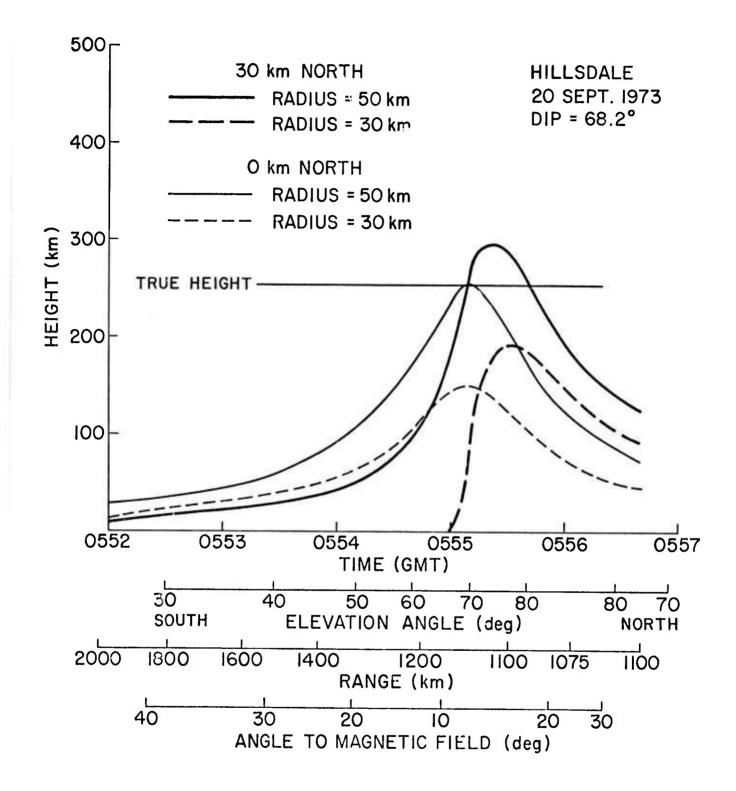
Figure 4.18 Cylinder model plot for Hillsdale, Wyo. pass
20 Sept. 1973
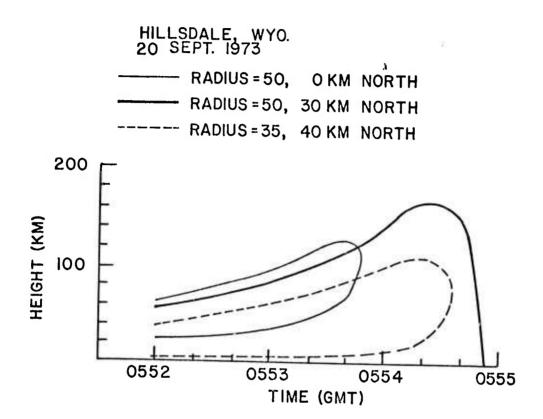
Figure 4.19   Cylinder model plot for Hillsdale, Wyo.
pass 20 Sept. 1973

multipath interference patterns should be seen in the amplitude versus time records for that time. A careful search of all available up-field orbital data has been made. No data containing the characteristic multipath interference pattern has been found.

4.6 Cimarron height variation

In order to study the variation of the heated region as a function of height, an orbital pass observation from 408 km geomagnetically south of the Platteville heater was made. This site, in Cimarron, New Mexico, was on a line extending normal to the magnetic field of the heated region (i.e., the cross field point).

Two satellites (on 27 and 28 September) moving from south to north were observed through the heated region. Figures 4.20 and 4.21 show the satellite signal amplitude as a function of time as the LOS passed through the heated region. Comparison of these data with the Hillsdale (down field) data has revealed some distinct differences. The scintillations at Hillsdale are deeper and more rapid than those seen at Cimarron. Also, it can be clearly seen that the signals from the three receivers at Hillsdale exhibit more similarity in the small-scale variations than the signals at Cimarron. Many of the peaks and nulls of the Hillsdale data are clearly seen in all three channels, but this is not true with the Cimarron data.

As an aid to interpretation of the data presented in Figures 4.20 and 4.21, the region of interest was modeled as a field-aligned cylinder. The projection of this cylinder on the 300-km-altitude plane is a circle which may be displaced to the magnetic north or south of overhead Platteville (Bowhill, et al., 1972, page 71). The altitude of the entry and exit of the satellite LOS from such cylinders is plotted as a function of time in Figures 4.22 and 4.23. The elevation angle and range from the observation point to the satellite as well as the angle of the LOS to the magnetic field over Platteville are also shown
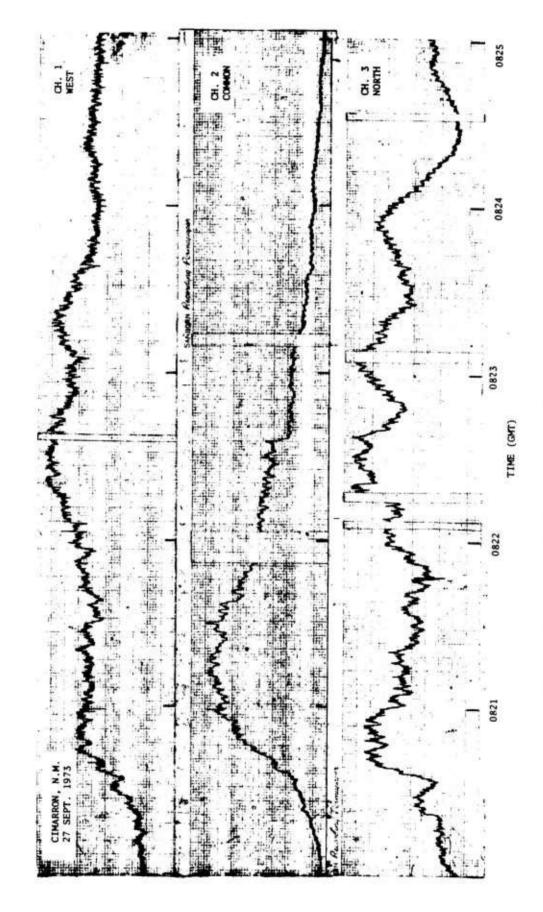
Figure 4.20 Signal amplitude at Cimarron, N.M. 27 Sept. 1973
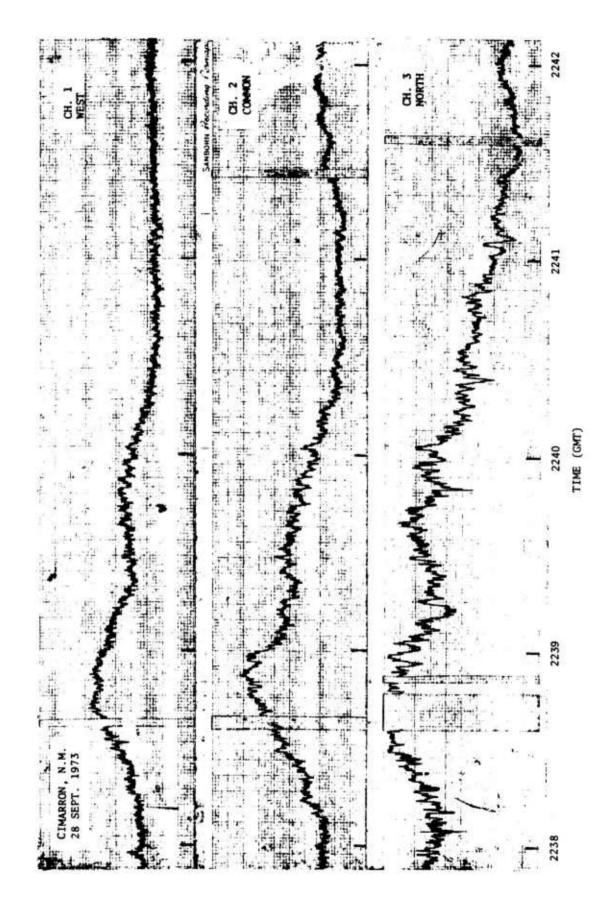
Figure 4.21 Signal amplitude at Cimarron, N.M. 28 Sept. 1973

82
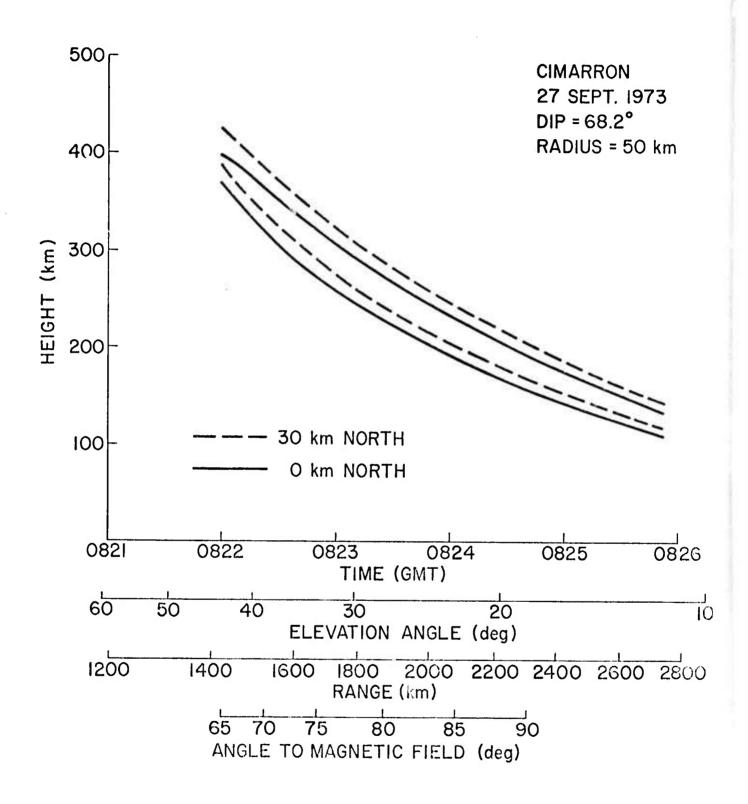
Figure 4.22 Cylinder model plot for Cimarron, N.M. 27 Sept. 1973
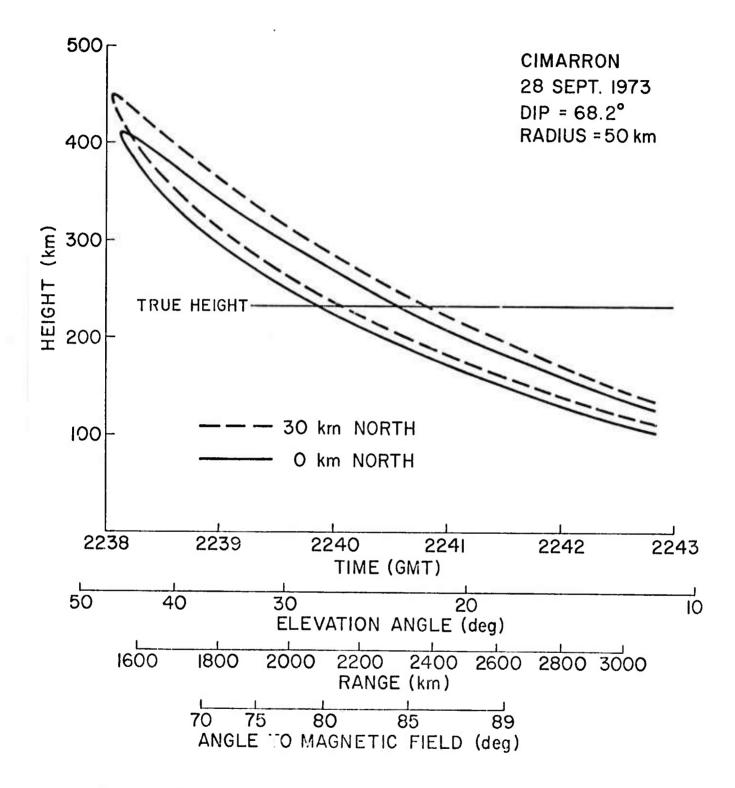
Figure 4.23 Cylinder model plot for Cimarron, N.M. 28 Sept. 1973

in these figures. Figure 4.23 also shows the true height of reflection for the transmitter frequency (provided by SRI). Figure 4.22 does not contain this true height due to the effect on foF2 of a magnetic disturbance for that day.

One would expect scintillations to occur when the LOS passed through the cylinder at regions near the true height of reflection of the heater transmitter signal.

Figure 4.24 shows the scintillation index versus time for the 28 September 1974 data. A description of the method used for obtaining these plots is given by Bowhill, et al. (1972).

The cross field location of the Cimarron site allows one to determine the vertical extent of the heated region by utilizing the scintillation index plots and the corresponding cylinder plot. To determine the height, a smoothed mean value curve of scintillation indices as well as a horizontal axis calibrated in average cylinder height for a field-aligned cylinder of 50-km radius located 30-km north of Platteville are displayed in Figure 4.24. It is evident that the heated region extends from approximately 340 km to 220 km. Note that the definition of the lower height is much sharper than that of the upper height as evidenced by a slow decrease in scintillation index in that region. The true height of reflection at f_H during this period was 232 km (f_c versus true-height data supplied by SRI).

4.7 Pulse compression

4.7.1 Theory

In order to obtain higher peak power in the ionosphere than the value due to maximum transmitter power, a pulse compression technique was suggested. This idea uses the time delay versus frequency characteristics of the ionosphere near the critical frequency. In this region, a small increase in frequency produces a large increase in the time required for the signal to reach the
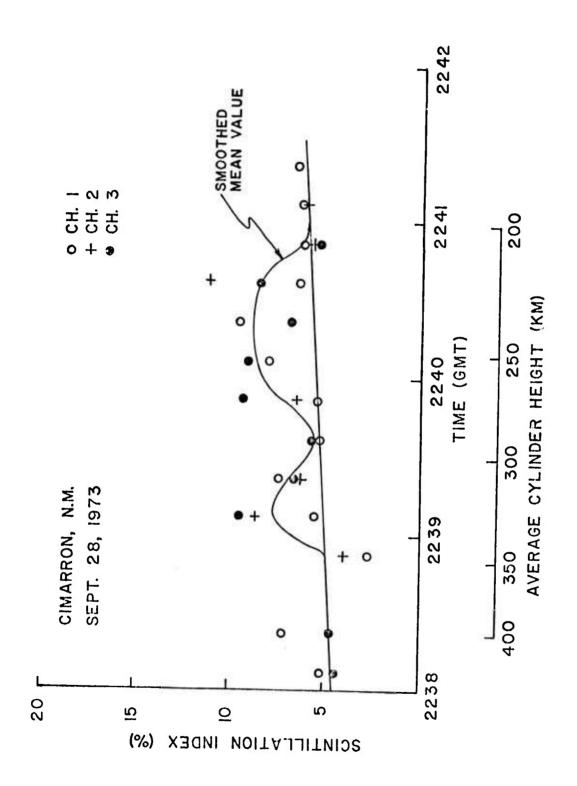
Figure 4.24 Scintillation index for Cimarron, N. M. pass 28 Sept. 1973

reflection level. The reflection level is assumed to be the level at which the heating effect is produced. The actual change in height near the critical frequency due to a frequency change is considerably less than the change in the virtual height (time delay) due to such a frequency change. To take advantage of this, a frequency sweep may be transmitted such that the higher frequencies are transmitted first, followed by the lower frequencies. The lower frequency components, with less time delay, might then "catch up" with the higher frequency components. In fact, if the frequency sweep is carefully chosen, the total signal could arrive at the height of reflection simultaneously, and deposit a pulse of energy much greater than the average energy available. The pulse compression experiment was performed in order to study the effect of such a frequency sweep scheme.

4.7.2 Experimental arrangement

In order to implement these ideas, the equipment shown in the block diagram of Figure 4.25 was set up. The bandwidth of the transmitters is 100 kHz, which limits the frequency range over which they can be swept. These transmitters are driven by an HP 5100A frequency synthesizer, which can be frequency swept using an applied dc voltage. It was modified so that it could be frequency swept at rates up to 10 kHz. A function generator was used to generate the voltage ramp and the offset bias such that the frequency sweep rate and extent of frequency shift as well as the average (center) frequency could be adjusted. The output of the function generator was monitored using an oscilloscope.

Once the equipment was set up, the operating procedure shown below was followed.

20 min before start time	Get h'(f) data from local VI ionosonde Plot data, Calculate T
1 min before start time	Get foF2 update and calculate operating frequency (96 to 99% foF2)

87
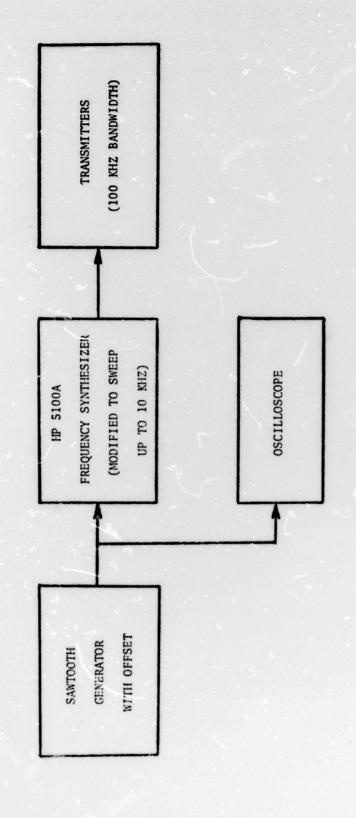
Figure 4.25 Pulse compression instrumentation

Start time	Set f_H as close to chosen operating frequency as possible. Operate with 5 transmitters, each at 1/2 power cw mode
Start time + 2 min	Sweep frequency 100 kHz in T sec (sawtooth)
Start time + 4 min	Sweep frequency 100 kHz in 120% of T sec (sawtooth)
Start time + 6 min	Sweep frequency 100 kHz in T sec (sawtooth)
Start time + 8 min	Sweep frequency 100 kHz in 80% of T sec (sawtooth)
Start time + 10 min	End of run.

The variable T is the time for the frequency to sweep downward 100 kHz. The retrace time was about 1/20 T. The value of T is calculated drawing a tangent to the h'(f) curve at $f = f_H$, and determining from the slope of this line the one-way time delay for a 100 kHz change. In order to cover a wide range of values for T, the value of f_H was chosen as 96% and 99% (in two cases) of foF2. The dates, times, and values of T and f_H used in this series of tests are listed in Table 4.2.

4.7.3 Results

In order to display how the sweep frequency program matched the slope of the virtual height curve at f_H, the series of ionograms shown in Figures 4.26 through 4.29 was prepared. Each ionogram was taken at the Erie site near Platteville during the pulse compression experiments. A line with slope equal to T(ms)/100 kHz, used during the experiment is drawn on each ionogram. The errors in the agreement between the slope of the line and the tangent to the ordinary mode trace are caused by two factors. One factor was the ionosphere itself. The critical frequency was changing rapidly or was difficult to determine (Figure 4.28, for example). A further problem was that the frequency of the transmitter cannot be chosen completely arbitrarily. Operation and legal restrictions prevented the frequency shown in Figures 4.26 and 4.29 from being set at the chosen value. As can be seen from the ionograms, the experiment performed

89

Table 4.2

Transmitter parameters during the Pulse Compression Experiment

Greenwich Mean Date	Start time	Desired f_H(MHz)	Actual f_H(MHz)	foF2(MHz)	%	T(ms)
Sept 11	18:26	5.70	5.949[1]	5.94	100	0.094
Sept 12	00:25	5.94	5.940	6.16	96	0.080
Sept 21	07:40	2.80	2.80	2.90	96	0.33
Sept 25	14:05	4.65	4.60[2]	4.77	96	0.47

[1]Unable to operate on 5.7 MHz. Closest frequency was 5.949 MHz.

[2]Unable to operate on 4.65 MHz. Closest frequency was 4.60 MHz.

The last two runs were planned to have f_H = 99% of foF2. Operational and legal restrictions prevented this.

18:30:00 GMT
11 SEPTEMBER, 1973

FREQUENCY (MHZ)

HEIGHT (KM)

f_H^6
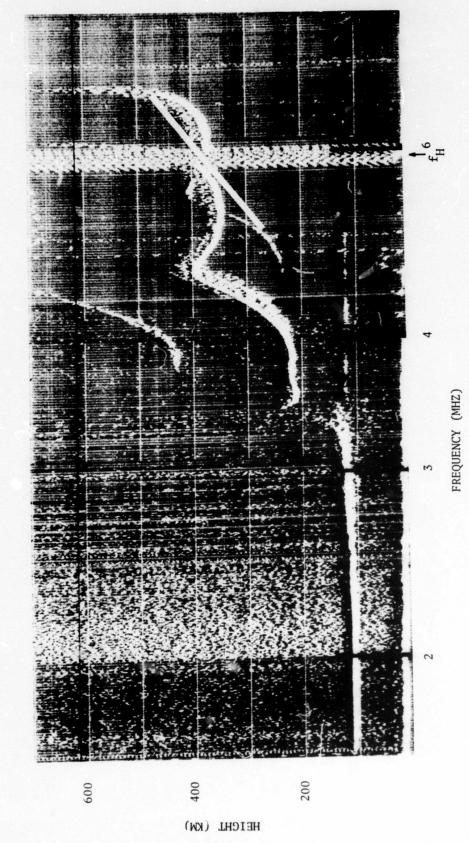
Figure 4.26   VI ionogram at Erie, Co. 11 Sept. 1973 18:30:00 GMT

00:29:59 GMT
12 SEPTEMBER, 1973
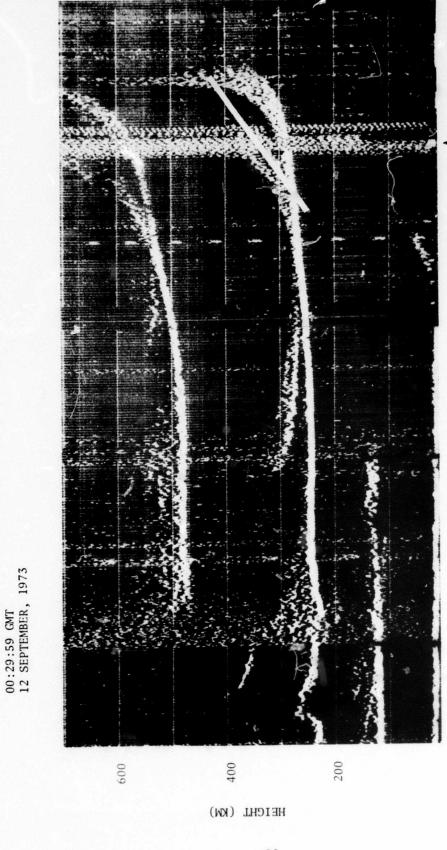
Figure 4.27 VI ionogram at Erie, Co. 12 Sept. 1973, 00:29:59 GMT

92

07:44:58 GMT
21 SEPTEMBER, 1973
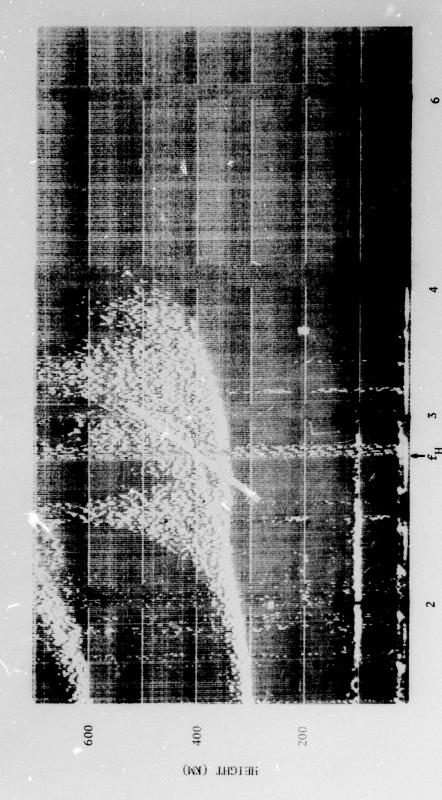
Figure 4.28 VI ionogram at Erie, Co. 21 Sept. 1973, 07:44:58 GMT

14:10:08 GMT
25 SEPTEMBER, 1973

FREQUENCY (MHZ)

HEIGHT (KM)
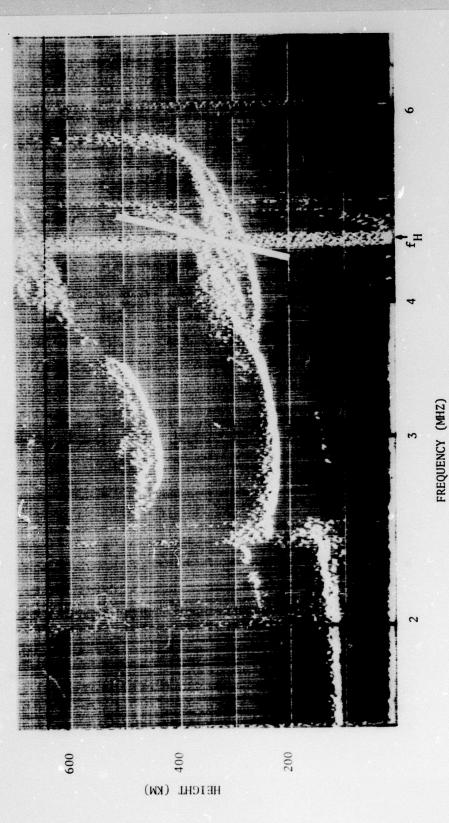
Figure 4.29 VI ionogram at Erie, Co. 25 Sept. 1973, 14:10:08 GMT

94

on September 12, 1973 (Figure 4.27) seems to have the best "match" as to ionospheric parameters.

Radar backscatter data are available for each of the experiments. The results are shown in Figures 4.30 through 4.33. The reduction in relative total cross section shown in Figures 4.30 and 4.31 may be accounted for by the reduction in transmitter power during the frequency sweep section of data. The -6 dB and -7 dB power measurements shown in Figure 4.30 were calculated from a 10-channel chart recording prepared at the Platteville transmitter site. Each of the ten transmitters has a forward power meter, and the dc voltage derived from these meters was recorded on 10-channel chart paper. Power calibration data for Figure 4.31 were taken from the SRI power monitor data. These data were provided by SRI in the form of a log of measured transmitter output. More accurate power calibration for the 21 September 1973 data is not available at this time.

It is clear from these plots that no significant change in the relative total cross section occurs due to the frequency sweeping performed during these experiments. This appears to indicate that the onset time of the ionospheric instability is comparable to, or larger than, the repetition time of the pulse compression wave form. Under these circumstances, it is essentially the average power which is seen, and the pulse compression does not produce an effective increase in yield.
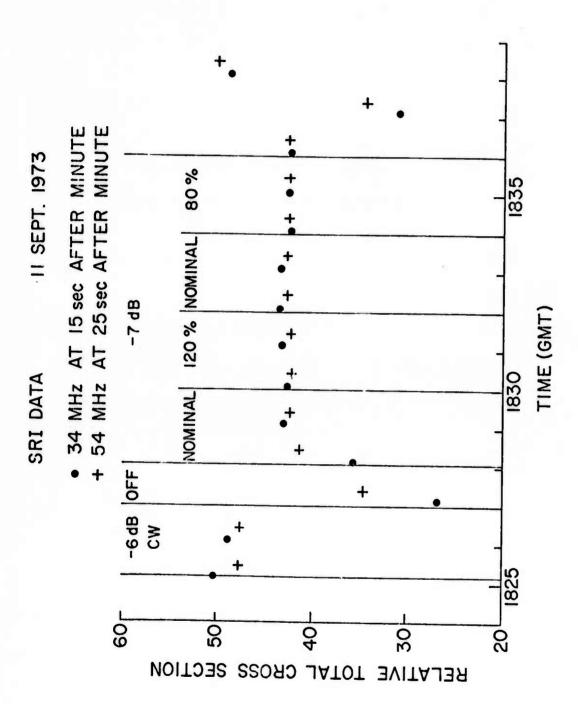
Figure 4.30   SRI radar backscatter data for 11 Sept. 1973

96

SRI DATA   12 SEPT. 1973 f_H = 5.94 MHZ = 96% foF2

O 55 MHZ   foF2 = 6.16 MHZ

● 75 MHZ

NOMINAL T = 0.08 MS

0.89 MW

OFF

0.38 MW
CW

0.19 MW
NOMINAL

0.19 MW
120%

0.19 MW
NOMINAL

0.19 MW
80%

RELATIVE TOTAL CROSS SECTION

70   60   50   40   30

0022   0024   0026   0028   0030   0032   0034   0036

TIME (GMT)
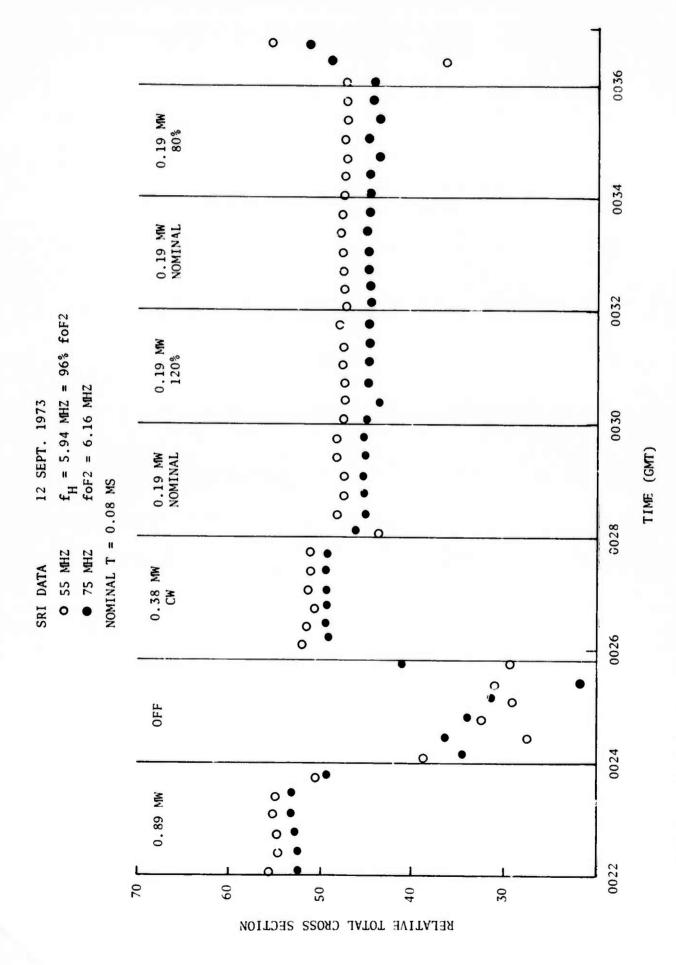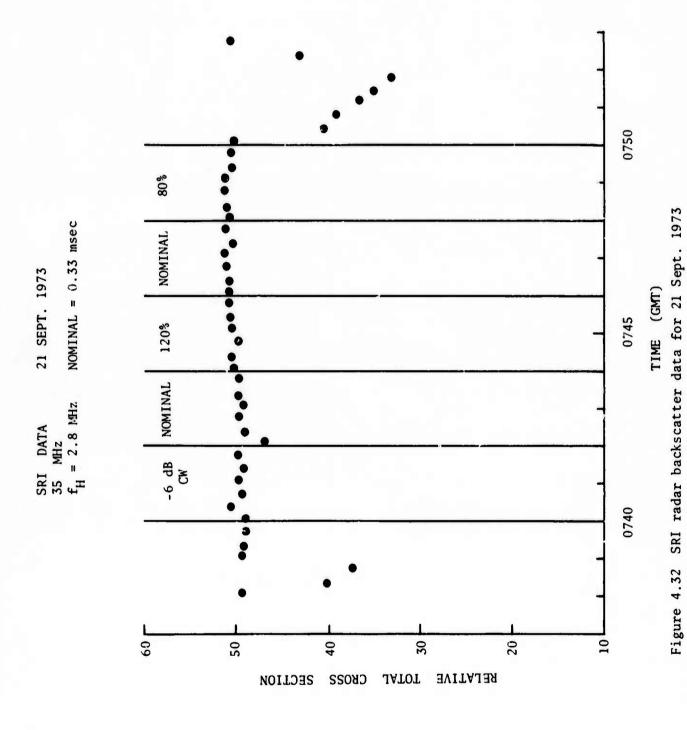
Figure 4.31 SRI radar backscatter data for 12 Sept. 1973

97

Figure 4.32 SRI radar backscatter data for 21 Sept. 1973
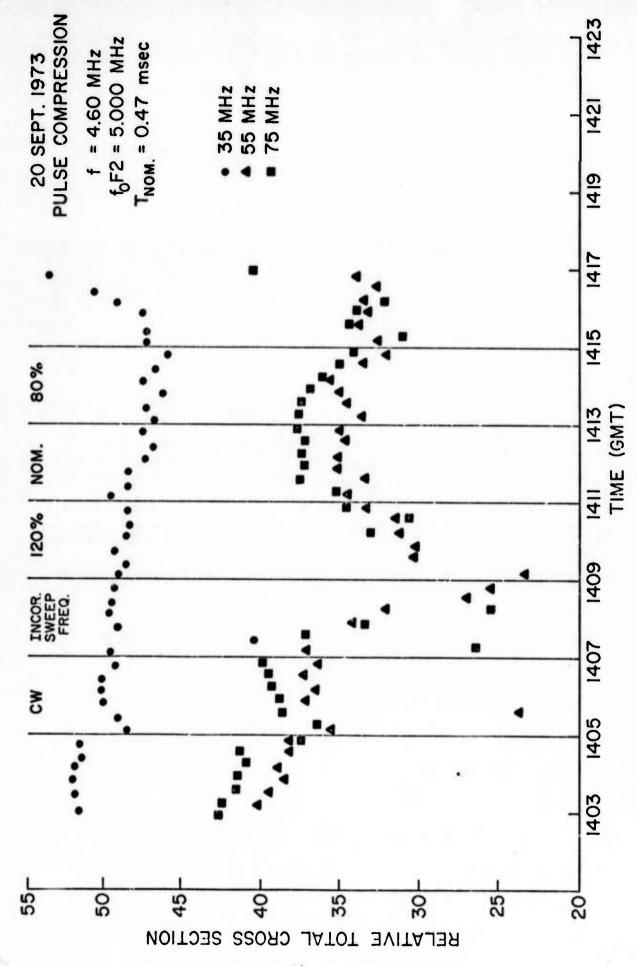
Figure 4.35 SRI radar backscatter data for 25 September 1973

5. SUMMARY

The Platteville ionospheric modification transmitter facility transmits on the order of 1.5 megawatts of power from a vertically-directed antenna array. The major effect of this intense RF heating is the production of large-scale field-aligned irregulatirites in ionization produced in the F layer described as artificial spread F (ASF). To clarify the reason for this description, the properties of naturally-occurring spread F (NSF) are briefly described, as are the characteristic differences between NSF and ASF. The properties of ASF are then combined into a single rational model suitable for systems-analysis purposes.

5.1 Natural spread F

NSF derives its name from the appearance produced on a sweep-frequency ionogram by irregularities in F-region ionization. These have been investigated extensively, and have indeed been the subject of a conference (Newman, 1966). While NSF has been classified into several distinct kinds, its mechanism of origin remains a mystery, as far as the temperate-latitude manifestations are concerned. Certain facts, on the other hand, seem fairly clear:

1. NSF is primarily a nighttime phenomenon, occurring to various degrees on perhaps 10-20 percent of nights at a typical mid-latitude station.

2. NSF tends to occur in patches several thousand kilometers in diameter, which seem to originate around magnetic latitude 60 deg and spread to lower latitudes.

3. The irregularities producing NSF are in the form of randomly arranged ellipsoidal enhancements or depletions of ionization, the principal axes of the ellipsoids being parallel to the local magnetic field direction, and the ellipsoids being centered approximately

100

on the F-region peak. In a horizontal direction, the electron-density profile has a random fluctuation with distance, the correlation function of the variation having an e-folding distance of about 1 km.

4. Parallel to the magnetic field, the enhancements or depletions of ionization continue through the F-region peak, and the fractional fluctuation in electron density seems to be approximately independent of altitude.

5. The spreading of ionosonde traces can be explained as due to trapping of obliquely incident signals in field-aligned ducts produced by the ionization depletions, causing the wave to be trapped and reflected at a range exceeding the normal range. This ducting is visible both from the bottom and topside (from sweep-frequency sounders on satellites).

5.2 Artificial spread F

The leading features of ASF may be compared with NSF as follows (using the same numbering as in Section 5.1):

1. ASF occurs on every occasion when ordinary-mode heating is used at a frequency slightly less than foF2. However, it appears to be more severe at night for the same heating power.

2. ASF occurs in an approximately circular region with radius about 50 km centered about 30 km north of the heater transmitter, with an onset and decay time of about a minute relative to the time of heating. The intensity of the irregularities is somewhat nonuniform in the horizontal direction, perhaps due to variations in the intensity of heating produced by gross horizontal inhomogeneities in the F layer.

3. As with NSF, the irregularities are field aligned with maximum intensity in the F-region peak. However, the e-folding distance of the horizontal correlation function of the structures is about one-tenth

101

of the natural scale; namely, about 100 m. The ASF irregularities
move horizontally with a few tens of m/s, apparently corresponding
to horizontal motions of the entire F layer.

4. As with NSF, the ASF irregularities continue all through the F layer
from 200 to about 450 km altitude. their intensity being approximately
proportional to the ambient electron density.

5.3 Transmission experiment results

Both the geostationary and orbital satellite transmission experiments
probed this ASF region. The geostationary data show that the disturbed region
contains approximately field-aligned irregularities moving in an east-west
direction with velocity 25 to 125 meters per second, and with essentially no
internal random motion. The observed correlation distance transverse to the
magnetic field varies from a daytime range of 100 to 250 km to a nighttime range
of 250 to 550 km.

The transmission experiment using orbiting satellites has been carried out
on a substantial number of satellite passes. Generally, ground observing points
have been selected so as to ensure that the LOS to the satellite traverses the
center of the disturbed region over the heater. If the satellite passes directly
over Platteville, it is possible to choose a site which looks directly upfield
through the disturbed region when the scintillation depth is greatest. However,
in general, the angle between the LOS and the magnetic field in the ionosphere goes
through a minimum value greater than zero, and the depth of fading is shallower,
the greater this minimum value. It is clear that the closer the LOS passes to
the magnetic field, the greater the depth of scintillation.

In making a close study of the cross correlation function of two spaced
antennas during an orbital pass, much finer structure was observed. Analysis
of this structure and the larger structure in conjunction shows that their
correlation distances appear to fluctuate together but with a ratio of approximately
20 to 1.

102

The conclusions are as follows:

1. The field-aligned structure gives strong VHF and UHF scintillations up to 400 MHz.

2. The scintillation index maximizes when the direction of propagation is close to the downfield direction. Therefore, for example, heating the ionosphere upfield from a radar will produce a "blind spot" of about 10 deg radius centered on the magnetic zenith at 150 MHz frequency.

3. The fading depth of the scintillation varies inversely with frequency, as would be expected from the integrated phase-path theory of satellite scintillations.

4. The transverse scale of the large-scale structure has a half-correlation distance of about 100 m, and convects in an east-west direction with velocity of the ambient plasma (about 20-50 m sec^{-1}).

5. The large-scale structure may extend from 200 to 450 km altitude, and is usually confined within a cylinder of about 50 km radius, with its axis parallel to the magnetic field line.

6. Occasionally, unusual shapes for the irregular region are seen, probably arising from a doughnut-shaped disturbed region due to burn-through of the central core of the ionosphere above the heater.

7. A finer-scale structure has been identified, with a scale size of 5-10 m, apparently centered close to the reflection height for the heater frequency. This structure is present for extraordinary-mode heating as well as for ordinary mode, but apparently with smaller intensity.

APPENDIX

A.1 Introduction

A description of the basic software developed for the analysis of orbital and geostationary transmission experiments is given here. The process can be divided into two parts, acquisition and analysis. For data acquisition, inputs were taken through an A/D converter of the PDP-8/3 minicomputer and from the interface to the Metrodata Type 622 digital magnetic tape reader. The data were stored on DECtape so that it could be easily accessed by analysis programs. The correlation analysis programs were written to allow flexibility in output and for maximum speed.

The hardware available for the work consisted of the following:

1. PDP-8/e central processing unit

2. Two DECtape drives with controller

3. A/D converter with 8-channel multiplexer, capable of approximately 40 Kz single channel sampling rate, resolution one part in 1024.

4. ASR-33 teletype for input/output

5. Three 4096 word memory banks (12,288 total words), 12 bits/word

6. OS/8 operating system containing an Editor, FORTRAN compiler, assembly language compiler

7. Metrodata 622 digital tape reader interfaced to PDP-8/e

A more detailed description (DEC, 1972a) is available giving speed and storage capabilities. The programming for this type of system needs to be compact since the memory is limited and large data arrays are necessary for analysis. This often leads to elaborate assembly-language programming even though arithmetic operations are difficult in this language.

Most of the programming was done in FORTRAN or SABR. The reader is referred to the proper handbook (DEC, 1972b) for details on these lanuguages. The FORTRAN

is basically a subset of FORTRAN II, and SABR is a relocatable machine code compiler.

A.2 Data acquisition

In order to process data available on analog tape, the data must first be digitized. Two programs that accept input from the A/D converter are DCOL and DCOL3. Both are written in FORTRAN and SABR, and are listed below. The program DCOL accepts a single channel of input and samples at a rate of 1 kHz for a total of 2000 samples. The start of sampling is controlled by the detection of a drop-out in the input signal. A synchronous drop-out in all channels was induced on the audio tape, and therefore samples of each channel would start at the same time. A single channel can be passed through a tracking filter, digitized, and correlated with another channel. The start of samples after a drop-out is a necessity for correlation analysis.

Three channels of input are accepted sequentially by DCOL3. Sychronization is no longer a problem since the channels are being sampled nearly simultaneously. Each channel is sampled at a rate of 1 kHz for a total of 1000 samples. Three separate files are written on DECtape under three names assigned by the user.

The files produced by these two programs are written onto DECtape by a FORTRAN write statement so that they can be accessed by FORTRAN read statements. The file organization is as follows:

> N number of samples in file
>> Sample 1
>> Sample 2
>> .
>> .
>> .
> Sample N

The number of samples is written as the first data point so that files of various length can be used. Since the output of the A/D converter is integer each sample takes only one word of storage. The format was chosen to achieve maximum packing density on the tape.

The final data acquisition program listed is called MDDTA which reads the digital Metrodata Type 622 reader and transfers the samples to DECtape. The programming is mostly SABR mixed with some FORTRAN. The programming is rather complex because the Metrodata delivers single characters to the accumulator and the logic must decide whether the character is parity or a digit. Three digits must be assembled into an integer and put into the proper channel for storage.

The files produced by MDDTA are of a different format than the other data files. Since three channels of data are available from the reader at once, the time to record three separate files onto DECtape would be long. A file structure in which the three channels are contained in one file was devised. The program reads, separates, and decodes from the Metrodata reader five minutes of data. The number of samples in a channel and the samples themselves are written into the files; this is repeated for the other two channels then five minutes more data are read and written onto DECtape until 30 minutes total data are read.

The file organization is as follows:

```
K number of samples in ch 1
      Sample 1
      Sample 2
         .
         .
         .
   Sample K

L number of samples in ch 2
      Sample 1
      Sample 2
         .
         .
         .
   Sample L

M number of samples in ch 3
      Sample 1
      Sample 2
         .
         .
   Sample M
         0
```

106

The final zero is used to signal the end of file. This example has one sweep of channels (1,2,3), but typically six sweeps were stored in one file with K=L=M=500. With this configuration 30 minutes of Metrodata output could be accomodated in one file.

These three programs are representative of the type of programming used for the data collection. The orbital experiment predominantly used the A/D converter routines, while the geostationary experiment utilized the Metrodata reader programs. A number of other programs were developed which are special variations of those presented here.

A.3 Correlation analysis

For data analysis, three basic programs are printed following this section, CCALH, CCALX, and METRO. All are written in FORTRAN and perform the correlation calculation on user specified files and intervals.

The basic core program upon which all other correlation programs were built is CCALH. The user inputs the data files to be correlated and the time shifts desired. The time shifts are performed at regular intervals (and in ascending order) because of the algorithm used to calculate the cross correlation. This algorithm computes the summations to calculate the correlation for the smallest time shift and then merely subtracts off those terms not needed for larger time shifts. For example, the cross correlation can be written as the expression

$$C_k = \frac{\frac{1}{N-k} \Sigma (A_j B_{j+k}) - \frac{1}{(N-k)^2} \Sigma A_j \, \Sigma B_{j+k}}{\left[\frac{1}{N-k} \Sigma (A_j)^2 - \frac{1}{N-k} \Sigma A_j{}^2\right]\left[\frac{1}{N-k} \Sigma (B_{j+k})^2 - \frac{1}{N-k} \Sigma B_{j+k}{}^2\right]^{1/2}}$$

where k is the shift and all the summations run from 1 to N-k. Suppose A and B contain 3 samples (N=3) and the correlation for k = 0 is calculated.

The various summations are as follows:

$$\Sigma A_j B_{j+k} = A_1 B_1 + A_2 B_2 + A_3 B_3$$

$$\Sigma A_j = A_1 + A_2 + A_3$$

$$\Sigma B_{j+k} = B_1 + B_2 + B_3$$

$$\Sigma (A_j)^2 = A_1^2 + A_2^2 + A_3^2$$

$$\Sigma (B_{j+k})^2 = B_1^2 + B_2^2 + B_3^2$$

For a shift of $k = 1$ the expressions become as follows:

$$\Sigma A_j B_{j+k} = A_1 B_2 + A_2 B_3$$

$$\Sigma A_j = A_1 + A_2$$

$$\Sigma B_{j+k} = B_2 + B_3$$

$$\Sigma (A_j)^2 = A_1^2 + A_2^2$$

$$\Sigma (B_{j+k})^2 = (B_2^2 + B_3^2)$$

The cross terms must be recalculated every time but the other summations are merely the previous summations with a term removed. This program utilizes this principle to speed up the calculation. If the time shifts are done in ascending order and at regular intervals a systematic formula for removing terms can be used. It should be noted that no gain in speed is obtained for the first time shift, but for many time shifts the gain is quite significant.

This program also has available two types of output, tabular or plot. The tabular printing is faster and the results are printed one time shift at a time. For the plot, all the time shifts are calculated, the minimum and maximum are found, and the plot is scaled appropriately. Therefore, there is a wait

108

during which all the calculations are being done. The plot enables trends in the data to be easily determined.

The second program CCALX is very similar to the first but it is able to read correctly the data file which contains three channels of data. The input is slightly different, but the actual calculation, printing, and plotting are identical to CCALH.

Subroutine CPLOT is used by CCALH and CCALX to plot the results. It searches the input data for minimum and maximum, and scales the data while being printed.

The final program (METRO) is the one which generated the correlation print-outs described in an earlier section. It was developed to provide automatic processing of files prepared from the Metrodata reader.

The program accepts a minimum of input, program name and calculation interval. A short paper tape can be prepared, and the computer can be left unattended for 10-12 hours calculating results. The program calculates the cross correlation of each possible pair of the three channels attempting to locate the peaks of the cross correlation curves. It contains logic which can deal with situations where the peak is in the reverse time shift or even where there is no peak at all. The autocorrelation of each channel is computed along with several statistical quantities to enable analysis for data quality.

The correlation calculation is identical to that of CCALH with different input, output, and logic to control the action of the program. There is no plot available, but the output is very comprehensive (for example see Section 3.3). This program was used in the velocity and structure size plots given in Section 3.2.

Finally, a number of other programs were developed to get results from the geostationary and orbital transmission experiments. One of the most important

109

was the calculation of scintillation index. The scintillation of orbital data was calculated in real-time during sampling of the analog tape. The scintillation of geostationary data was calculated from the data files stored on DECtape. Other versions of the correlation programs were used at various times, but the ones printed here represent the latest and most efficient algorithms. The software development was a continuing effort throughout the work period.

DIGITIZATION PROGRAM
(1-channel)

```
C DCOL.FT
C IDENTIFIES A DIP IN INPUT SIGNAL TO AD CHANNEL 0
C BEGINS COLLECTING SAMPLES A SHORT TIME AFTER THE DIP ENDS
C THE AMOUNT OF DIP DETECTED IS VARIABLE BY USER INPUT
C 2000 SAMPLES AT 1000 SAMPLES/SEC, TOTAL OF 2 SECONDS INPUT
C
S         OPDEF ADLM 6531
S         OPDEF ADST 6532
S         OPDEF ADRB 6533
S         SKPDF ADSK 6534
          DIMENSION IS(2000)
5         WRITE(1,9)
9         FORMAT(' DATAFILE NAME')
          READ(1,10) FNAME
10        FORMAT(A6)
          CALL OOPEN('DTA1',FNAME)
          WRITE(1,11)
11        FORMAT(' THRESHOLD FOR START')
          READ(1,12) LDIP
12        FORMAT(I2)
14        ID=0
S         CLA
S         ADLM
          PAUSE
15        CONTINUE
S         ADST
S ASK,    ADSK
S         JMP ASK
S         ADRB
S         DCA \IT
          IF(IT-LDIP) 16,16,51
16        ID=1
          GO TO 15
51        IF(ID) 15,15,52
52        DO 55 K=1,50
S         ADST
S BSK,    ADSK
S         JMP BSK
S         ADRB
S         DCA \IT
          DO 31 L=1,50
31        CONTINUE
55        CONTINUE
          DO 41 K=1,2000
S         ADST
S SK,     ADSK
S         JMP SK
S         ADRB
S         DCA \IT
          IS(K)=IT
          DO 32 L=1,30
32        CONTINUE
41        CONTINUE
```

DIGITIZATION PROGRAM (Cont'd)
(1-channel)

```
       WRITE(1,42)
42     FORMAT(' OK=0 ')
       READ(1,43) NTRY
43     FORMAT(I2)
       IF(NTRY) 14,44,14
44     CONTINUE
       K=K-1
       WRITE(4,45) K
45     FORMAT(A2)
       WRITE(4,50) (IS(N),N=1,2000)
50     FORMAT(100A2)
       CALL CCLOSE
       GO TO 5
       END
```

DIGITIZATION PROGRAM (3-channel)

```
C DCOL3.FT
C 3 CHANNELS ARE SEQUENTIALLY SAMPLED, FOR A TOTAL OF 1000 SAMPLES
C FOR EACH CHANNEL
C
S          OPDEF ADLE 6536
S          OPDEF ADLM 6531
S          OPDEF ADCL 6530
S          OPDEF ADST 6532
S          OPDEF ADRB 6533
S          SKPDF ADSK 6534
           DIMENSION ISA(1000),ISB(1000),ISC(1000),FNAM(3)
5          CONTINUE
           WRITE(1,9)
9          FORMAT(' DATAFILE NAME',/,7X,':',6X,':')
           READ(1,10) (FNAM(K),K=1,3)
10         FORMAT(3(A6,1X))
100        ITA=64
S          ADCL
S          CLA
S          TAD \ITA
S          ADLE
           PAUSE
15         CONTINUE
           DO 41 K=1,1000
S          CLA
S          ADLM
S          ADST
S SK,      ADSK
S          JMP SK
S          ADRB
S          DCA \ITA
S          ADST
S SKA,     ADSK
S          JMP SKA
S          ADRB
S          DCA \ITB
S          ADST
S SKB,     ADSK
S          JMP SKB
S          ADRB
S          DCA \ITC
           ISA(K)=ITA
           ISB(K)=ITB
           ISC(K)=ITC
41         CONTINUE
           IAMX=ISA(1)
           IBMX=ISB(1)
           ICMX=ISC(1)
           DO 70 N=2,1000
           IF(IAMX-ISA(N)) 72,74,74
72         IAMX=ISA(N)
74         IF(IBMX-ISB(N)) 76,78,78
76         IBMX=ISB(N)
78         IF(ICMX-ISC(N)) 80,70,70
80         ICMX=ISC(N)
70         CONTINUE
```

113

```
        AMX=FLOAT(IAMX)*1000./511.
        BMX=FLOAT(IBMX)*1000./511.
        CMX=FLOAT(ICMX)*1000./511.
        WRITE(1,85) AMX,BMX,CMX
85      FORMAT(F6.0,1X,F6.0,1X,F6.0,'  MAX INPUT (MV)')
        WRITE(1,90)
90      FORMAT(' CR TO ACCEPT')
        READ(1,91) ITA
91      FORMAT(I2)
        IF(ITA) 100,92,100
92      K=1000
        DO 55 L=1,3
        FNM=FNAM(L)
        CALL OOPEN('DTA1',FNM)
        WRITE(4,45) K
45      FORMAT(A2)
        IF(L-2) 56,57,58
56      WRITE(4,50) (ISA(N),N=1,1000)
        GO TO 55
57      WRITE(4,50) (ISB(N),N=1,1000)
        GO TO 55
58      WRITE(4,50) (ISC(N),N=1,1000)
55      CALL OCLOSE
50      FORMAT(100A2)
        GO TO 5
        END
```

```
          DIMENSION IS(3,500)
1         WRITE(1,10)
10        FORMAT(' NUMBER OF 5 MIN. BLOCKS')
          READ(1,11) IBLK
11        FORMAT(I2)
          ICB=0
S         CLA
S         TAD \IBLK
S         CIA
S         DCA \IBLK
          WRITE(1,5)
5         FORMAT(' DATAFILE NAME ')
          READ(1,6) FNAM
6         FORMAT(A6)
          CALL OOPEN('DTAI',FNAM)
S OPDEF MSTR 6141
S OPDEF MTAD 6142
S SKPDF MSKP 6143
S OPDEF MSTP 6144
S OPDEF MRST 6145
S RST,   CLA
S         TAD M750
S         DCA BCNT
S         TAD M96
S         DCA CM96
S         DCA \K
S         INC \K
S         DCA \CNL
S         INC \CNL
S         MRST
S         MSTR
S REDM,   MSKP
S         JMP REDM
S         MTAD
S         ISZ CM96
S         JMP REDM
S READ,   MSKP
S         JMP READ
S         MTAD
S DTST,   TAD M12
S         SMA
S         JMP READ
S DA,     MSKP
S         JMP DA
S         MTAD
S         TAD M14
S         SMA
S         JMP SP
S         TAD P14
S         JMP DTST
S SP,     CLA
S         TAD M1
S         DCA RDSK
S         JMS SKCH
```

115

METRODATA PROGRAM (Cont'd)

```
S CONTL,MSKP
S          JMP CONTL
S          MTAD
S          TAD M12
S          SZA
S          JMP AHD
S          CLA
S          TAD (7000
S          DCA SWT
S          JMP DIG
S AHD,     TAD P12
S          TAD M13
S          SZA
S          JMP ERR
S          CLA
S          TAD (7041
S          DCA SWT
S DIG,     TAD M3
S          DCA CDG
S          DCA TS
S RDG,     MSKP
S          JMP RDG
S          MTAD
S          TAD M12
S          SMA
S          JMP ERR
S          TAD P12
S          TAD TS
S          DCA TS
S          ISZ CDG
S          JMP MUL10
S          CLA
S          TAD TS
S SWT,     NOP
S          DCA \IT
           IS(CNL,K)=IT
S          INC \CNL
S          CLA
S          TAD \CNL
S          TAD M4
S          SZA
S          JMP CONTL
S          CLA
S          DCA \CNL
S          INC \CNL
S          INC \K
S          CLA
S          TAD M6
S          DCA RDSK
S          JMS SKCH
S          ISZ BCNT
S          JMP CONTL
S          MSTP
S          CLA
```

```
            CONTINUE
            ICB=ICB+1
            WRITE(1,11) ICB
            NS=500
            DO 70 I=1,3
            WRITE(4,20) NS
20          FORMAT(A2)
            WRITE(4,30) (IS(I,L),L=1,500)
30          FORMAT(100A2)
70          CONTINUE
S           ISZ \IBLK
S           JMP RST
S           NOP
            NS=0
            WRITE(4,20) NS
            CALL OCLOSE
            GO TO 1
S MUL10,CLA
S           TAD TS
S           CLL
S           RAL
S           DCA TS
S           TAD TS
S           CLL
S           RTL
S           TAD TS
S           DCA TS
S           JMP RDG
S SKCH,  0
S SKA,   MSKP
S           JMP SKA
S           MTAD
S           ISZ RDSK
S           JMP SKA
S           JMP I SKCH
C
S ERR,   MSTP
            WRITE(1,60) K
60          FORMAT(' ERROR AT ',I3)
S           JMP RST
S M750,  7014
S BCNT,  0
S M12,   7766
S M14,   7764
S M1,    7777
S M13,   7765
S M3,    7775
S P12,   12
S TS,    0
S CDG,   0
S RDSK,  0
S M6,    7772
S M96,   7640
S CM96,  0
S M4,    7774
S P14,   14
            END                    117
```

```
C CCALH.FT
C STREAMLINED CROSS-CORRELATION CALCULATION
C ASSUMES INPUT ARRAYS ARE SAME SIZE AND LESS THAN OR EQUAL
C TO 2000 IN SIZE
C INPUTS ARE ARRAY FILENAMES, STARTING TIME SHIFT, INCREMENT OF
C THE TIME SHIFT, AND THE NUMBER OF TIME SHIFTS DESIRED
C INSERTING A NEGATIVE NUMBER OF TIME SHIFTS CAUSES THE
C SENSE OF THE SHIFT TO BE REVERSED
C
          COMMON IA
          DIMENSION IA(2000),IB(2000),IC(200)
1         WRITE(1,10)
10        FORMAT(' DATAFILES')
          READ(1,20) ANAME,BNAME
20        FORMAT(A6)
          WRITE(1,30)
30        FORMAT(' TIME SHIFT',/,' START,INCREMENT,NUMBER')
          READ(1,40) KO,KI,NK
40        FORMAT(I3)
          WRITE(1,41)
41        FORMAT(' PLOT - Y OR N')
          READ(1,42) JRSP
42        FORMAT(A1)
          JRSP=JRSP-1631
          NK=IABS(NK)
          CALL IOPEN('DTA1',ANAME)
          READ(4,50) NSIZ
50        FORMAT(A2)
          READ(4,60) (IA(L),L=1,NSIZ)
60        FORMAT(100A2)
          CALL IOPEN('DTA1',BNAME)
          READ(4,50) NSIZ
          READ(4,60) (IB(L),L=1,NSIZ)
          WRITE(1,70) NSIZ
70        FORMAT(' ARRAY SIZE ',I4)
90        K=KO
          IDM=NSIZ-K
          SA=0.
          SA2=0.
          SB=0.
          SB2=0.
          DO 105 L=1,IDM
          KB=L+K
          Y=FLOAT(IA(L))
          SA=SA+Y
          SA2=SA2+Y*Y
          Z=FLOAT(IB(KB))
          SB=SB+Z
          SB2=SB2+Z*Z
105       CONTINUE
          DO 140 M=1,NK
          KM=KI*(M-1)
          KMP=KI*(M-2)
          IF(M-1)17,17,18
```

```
18        DO 120 J=1,KI
          KA=IDM-KMP-J+1
          XDUM=FLOAT(IA(KA))
          SA=SA-XDUM
          SA2=SA2-XDUM*XDUM
          KB=K+KMP+J
          XDUM=FLOAT(IB(KB))
          SB=SB-XDUM
          SB2=SB2-XDUM*XDUM
120       CONTINUE
17        X=FLOAT(IDM-KM)
          FN=SQRT((X*SA2-(SA*SA))*(X*SB2-(SB*SB)))
          XAB=0.
          NUM=IDM-KM
          DO 133 I=1,NUM
          III=K+KM+I
          XAB=XAB+FLOAT(IA(I))*FLOAT(IB(III))
133       CONTINUE
          C=(X*XAB-SA*SB)/FN
          KCUR=K+KI*(M-1)
          IF(JRSP) 201,201,202
201       WRITE(1,191) KCUR,C
191       FORMAT(I3,3X,F10.5)
          GO TO 140
202       IC(M)=C*1000.
140       CONTINUE
          IF(JRSP) 203,203,204
204       CALL CPLOT(IC,KO,KI,NK)
203       WRITE(1,30)
          READ(1,40) KO,KI,NK
          IF(NK) 150,1,90
150       DO 160 L=1,NSIZ
          IDM=IA(L)
          IA(L)=IB(L)
          IB(L)=IDM
160       CONTINUE
          NK=-NK
          GO TO 90
          END
```

```
CORRELATION PROGRAM VERSION B
C CCALX.FT
C USES X-PREFIX FILES ONLY, AND ASSUMES 3 CHANNELS PER FILE
C STREAMLINED CROSS-CORRELATION CALCULATION
C ASSUMES INPUT ARRAYS ARE SAME SIZE AND LESS THAN OR EQUAL
C TO 2000 IN SIZE
C INPUTS ARE ARRAY FILENAMES, STARTING TIME SHIFT, INCREMENT OF
C THE TIME SHIFT, AND THE NUMBER OF TIME SHIFTS DESIRED
C INSERTING A NEGATIVE NUMBER OF TIME SHIFTS CAUSES THE
C SENSE OF THE SHIFT TO BE REVERSED
C
          COMMON IA
          DIMENSION IA(2000),IB(2000),IC(200)
1         WRITE(1,10)
10        FORMAT(' DATAFILE')
          READ(1,20) ANAME
20        FORMAT(A6)
          WRITE(1,22)
22        FORMAT(' CHANNELS')
          READ(1,24) IACH,IBCH
24        FORMAT(I2)
          WRITE(1,302)
302       FORMAT(' INTERVAL NUMBER')
          READ(1,24) NFM
          WRITE(1,30)
30        FORMAT(' TIME SHIFT',/,' START,INCREMENT,NUMBER')
          READ(1,40) KO,KI,NK
40        FORMAT(I3)
          WRITE(1,41)
41        FORMAT(' PLOT - Y OR N')
          READ(1,42) JRSP
42        FORMAT(A1)
          JRSP=JRSP-1631
          NK=IABS(NK)
          CALL IOPEN('DTA1',ANAME)
          DO 301 K=1,NFM
          DO 51 J=1,3
          READ(4,50) NSIZ
50        FORMAT(A2)
          IF(J-IACH) 53,52,53
52        READ(4,60) (IA(L),L=1,NSIZ)
60        FORMAT(100A2)
          GO TO 51
53        IF(J-IBCH) 54,55,54
55        READ(4,60) (IB(L),L=1,NSIZ)
          GO TO 51
54        READ(4,60) (IDUM,L=1,NSIZ)
51        CONTINUE
301       CONTINUE
          IF(IACH-IBCH) 62,61,62
61        DO 63 J=1,NSIZ
          IB(J)=IA(J)
63        CONTINUE
62        CONTINUE
          WRITE(1,70) NSIZ
70        FORMAT(' ARRAY SIZE ',I4)
93        K=KO
          IDM=NSIZ-K
```

```
            SA=0.
            SA2=0.
            SB=0.
            SB2=0.
            DO 105 L=1,IDM
            KB=L+K
            Y=FLOAT(IA(L))
            SA=SA+Y
            SA2=SA2+Y*Y
            Z=FLOAT(IB(KB))
            SB=SB+Z
            SB2=SB2+Z*Z
105         CONTINUE
            DO 140 M=1,NK
            KM=KI*(M-1)
            KMP=KI*(M-2)
            IF(M-1)17,17,18
18          DO 120 J=1,KI
            KA=IDM-KMP-J+1
            XDUM=FLOAT(IA(KA))
            SA=SA-XDUM
            SA2=SA2-XDUM*XDUM
            KB=K+KMP+J
            XDUM=FLOAT(IB(KB))
            SB=SB-XDUM
            SB2=SB2-XDUM*XDUM
120         CONTINUE
17          X=FLOAT(IDM-KM)
            FN=SQRT((X*SA2-(SA*SA))*(X*SB2-(SB*SB)))
            XAB=0.
            NUM=IDM-KM
            DO 133 I=1,NUM
            III=K+KM+I
            XAB=XAB+FLOAT(IA(I))*FLOAT(IB(III))
133         CONTINUE
            C=(X*XAB-SA*SB)/FN
            KCUR=K+KI*(M-1)
            IF(JRSP) 201,201,202
201         WRITE(1,191) KCUR,C
191         FORMAT(I3,3X,F10.5)
            GO TO 140
202         IC(M)=C*1000.
140         CONTINUE
            IF(JRSP) 203,203,204
204         CALL CPLOT(IC,KO,KI,NK)
203         WRITE(1,30)
            READ(1,40) KO,KI,NK
            IF(NK) 150,1,90
150         DO 160 L=1,NSIZ
            IDM=IA(L)
            IA(L)=IB(L)
            IB(L)=IDM
160         CONTINUE
            NK=-NK
            GO TO 90
            END
```

PLOTTING SUBROUTINE USED WITH CORRELATION PROGRAMS

```
        SUBROUTINE CPLOT(IC,KO,KI,NK)
        DIMENSION IC(1)
        ISTAR=-1376
        IZIP=-2016
        K=KO
        IMIN=IC(1)
        IMAX=IC(1)
        DO 3 M=2,NK
        IF(IC(M)-IMIN) 1,2,2
2       IF(IC(M)-IMAX) 3,3,4
1       IMIN=IC(M)
        GO TO 3
4       IMAX=IC(M)
3       CONTINUE
        WRITE(1,101) IMIN,IMAX
101     FORMAT(10X,I4,18X,'CORRELATION',17X,I5)
        DELT = IMAX-IMIN
        DO 5 M=1,NK
        SPAS=50.0*(FLOAT(IC(M) -IMIN))/DELT
        ISPAS =SPAS
        WRITE(1,102) K,IC(M),(IZIP,J=1,ISPAS),ISTAR
        K=K+KI
102     FORMAT(I4,I6,' :',51A1)
5       CONTINUE
        RETURN
        END
```

AUTOMATIC CORRELATION PROCESSING PROGRAM

```
C METRO.FT
C AUTOMATIC PROCESSING OF X-PREFIX FILES
C GIVES CROSS- AND AUTO-CORRELATION
C ALSO COMPUTES SCINTILLATION INDEX, STANDARD DEVIATION, AND MEAN
C ASSUMES FILES CONSIST OF 6 FIVE MINUTE INTERVALS, 3 CHANNELS
C
          DIMENSION IA(3,500),KCC(300),LM(10),LN(10),X1(3),X2(3)
          LM(1)=1
          LN(1)=2
          LM(2)=2
          LN(2)=1
          LM(3)=2
          LN(3)=3
          LM(4)=3
          LN(4)=2
          LM(5)=1
          LN(5)=3
          LM(6)=3
          LN(6)=1
          LM(7)=1
          LN(7)=1
          LM(8)=2
          LN(8)=2
          LM(9)=3
          LN(9)=3
10        WRITE(1,20)
20        FORMAT(' DATAFILE, INTERVAL ')
          READ(1,30) FNAM,INC
30        FORMAT(A6,'   ',I2)
          INTV=0
          CALL IOPEN('DTA1',FNAM)
40        MIN=1000
          JA=0
          INTV=INTV+1
          WRITE(1,50) FNAM,INTV
50        FORMAT(/,3X,A6,' PART ',I2)
          KTEST=1001
          NN=1
          JMP=1
          DO 80 LL=1,3
          READ(4,60) NSIZ
60        FORMAT(A2)
          NSIZ=500
          READ(4,70) (IA(LL,L),L=1,NSIZ)
70        FORMAT(100A2)
80        CONTINUE
90        NCC=1
100       M=LM(NN)
          N=LN(NN)
C
C CROSS-CORRELATION CALCULATION
110       K=(NCC-1)*INC
          IDM=NSIZ-K
```

```
              SA=0.
              SA2=0.
              SF=0.
              SB2=0.
              DO 120 L=1,IDM
              KB=L+K
              Y=FLOAT(IA(M,L))
              SA=SA+Y
              SA2=SA2+Y*Y
              Z=FLOAT(IA(N,KB))
              SB=SB+Z
              SB2=SB2+Z*Z
120           CONTINUE
              IF(NCC-1) 140,130,140
130           FNSIZ=FLOAT(NSIZ)
              X1(M)=SA/FNSIZ
              X2(M)=SQRT(SA2/FNSIZ-X1(M)*X1(M))
              X1(N)=SB/FNSIZ
              X2(N)=SQRT(SB2/FNSIZ-X1(N)*X1(N))
140           CONTINUE
              GO TO 170
C RESTART ENTRY
150           DO 160 J=1,INC
              KA=NSIZ-(NCC-1)*INC+J
              XDUM=FLOAT(IA(M,KA))
              SA=SA-XDUM
              SA2=SA2-XDUM*XDUM
              KB=(NCC-1)*INC-J+1
              XDUM=FLOAT(IA(N,KB))
              SB=SB-XDUM
              SB2=SB2-XDUM*XDUM
160           CONTINUE
170           NUM=NSIZ-(NCC-1)*INC
              X=FLOAT(NUM)
              FN=SQRT((X*SA2-(SA*SA))*(X*SB2-(SB*SB)))
              XAB=0.
              DO 180 I=1,NUM
              III=(NCC-1)*INC+I
              XAB=XAB+FLOAT(IA(M,I))*FLOAT(IA(N,III))
180           CONTINUE
              CC=(X*XAB-SA*SB)/FN
              KCC(NCC)=CC*1000.
190           IF(KCC(NCC)-KTEST) 240,200,200
200           JMP=4+JA
210           NCC=NCC+1
              IF(NCC*INC-100) 150,150,220
220           WRITE(1,230)
230           FORMAT(' OUT OF RANGE')
240           JA=NN/7
              GO TO (501,502,503,504,505),JMP
C
C
501           JMP=2
              KTEST=KCC(1)
              GO TO 210
C
```

124

```
C
502       JMP=3
          NN=NN+1
          WRITE(1,250) M,N,KCC(1),KCC(2)
250       FORMAT(' BACKSIDE',2I3,2X,2I6)
          GO TO 100
C
C
503       WRITE(1,260) M,N,KCC(1),KCC(2)
260       FORMAT(' NO TIME SHIFT',4I6)
          NN=NN+1
          KTEST=1001
          JMP=1
270       IF(KCC(1)-MIN) 280,290,290
280       MIN=KCC(1)
290       IF(NN-7) 90,300,300
300       KTEST=MIN
          JA=1
          NCC=2
          JMP=5
          GO TO 100
C
C
504       WRITE(1,310) M,N,INC,(KCC(L),L=1,NCC)
310       FORMAT(3I8,/,(10I6))
          IF(NN-4) 330,330,320
320       NN=7
          GO TO 270
330       IF(NN-2) 340,340,350
340       NN=3
          GO TO 360
350       NN=5
360       JMP=1
          KTEST=1001
          GO TO 270
C
C
505       X3=100.*X2(M)/X1(M)
          WRITE(1,370) M,M,INC,X1(M),X2(M),X3
370       FORMAT(3I4,' MEAN ',F6.0,' STD DEV ',F6.0,'SCINT ',
         1 F6.1,'%')
          WRITE(1,380) (KCC(L),L=2,NCC)
380       FORMAT(10I6)
          NN=NN+1
          IF(NN-10) 390,400,400
390       NCC=2
          GO TO 100
400       IF(INTV-6) 40,10,10
          END
```

REFERENCES

Bowhill, S. A., IVORY CORAL applications and diagnostics (U), RADC TR 72-254, 1971 (AD523 292)

Bowhill, S. A., E. E. Mendenhall, and D. R. Ward, "Transmission experiments in Prairie Smoke II RF Measurements Data Workshop--22, 23 June 1972 (U)", SRI 25388, Stanford Research Institute, Menlo Park, CA (October 1972)

Bowhill, S. A., E. E. Mendenhall, and D. R. Ward, Experiements and models in Prairie Smoke, RADC TR-73-210, April 1973 (AD527 361)

Bowhill, S. A., N. N. Rao, and E. E. Mendenhall, Diagnostic experiments for IVORY CORAL (U), RADC TR-71-247, (January 1971) (AD518 713)

Bowhill, S. A. and D. R. Ward, "Geostationary transmission experiments in Prairie Smoke·IV (U)", in Proceedings of the Prairie Smoke IV RF Measurements Data Workshop, 7 March 1973 (U), SRI 3-4836, Stanford Research Institute, Menlo Park, CA (June 1973a)

Bowhill, S. A. and D. R. Ward "Correlation analysis of Prairie Smoke transmission results (U)", in Proceedings of the Prairie Smoke IV RF Measurements Data Workshop, 7 March 1973 (U), SRI 3-4836, Stanford Research Institute, Menlo Park, CA (June 1973b)

Briggs, G. H. and I. A. Parkin, On the variation of radio star and satellite scintillations with zenith angle, J. Atmosph. Terr. Phys. 25, 339-365 (1973)

Briggs, B. H., G. J. Phillips and D. H. Shinn, Proc. Phys. Soc. B, 63, 106 (1950)

Newman, P., Spread F and its effects upon radio wave propagation and communication, AGARDograph 95, Technivision, Maidenhead, England, 579-590 (1966)

Digital Equipment Corporation, PDP-8/e and PDP-8/m Small Computer Handbook, Maynard, MA (1972a)

Digital Equipment Corporation, Programming Languages, Maynard, MA (1972b)

Walton, E. K., D. R. Ward, and S. A. Bowhill, "Yield studies based on geo-stationary-satellite transmissions (U)", in Proceedings of the Prairie Smoke Yield-Model Workshop 17, 18 July 1973 (U), SRI 3-5193, Stanford Research Institute, Menlo Park, CA (October 1973)

MISSION
of
Rome Air Development Center

RADC is the principal AFSC organization charged with planning and executing the USAF exploratory and advanced development programs for information sciences, intelligence, command, control and communications technology, products and services oriented to the needs of the USAF. Primary RADC mission areas are communications, electromagnetic guidance and control, surveillance of ground and aerospace objects, intelligence data collection and handling, information system technology, and electronic reliability, maintainability and compatibility. RADC has mission responsibility as assigned by AFSC for demonstration and acquisition of selected subsystems and systems in the intelligence, mapping, charting, command, control and communications areas.